SANDIA REPORT
SAND2006-3494
Unlimited Release
Printed June 2006

Validation Experiments to Determine Radiation Partitioning of Heat Flux to an Object in a Fully Turbulent Fire

Allen Ricks, Thomas Blanchat, and Dann Jernigan

Prepared by
Sandia National Laboratories
Albuquerque, New Mexico 87185 and Livermore, California 94550

Sandia is a multiprogram laboratory operated by Sandia Corporation,
a Lockheed Martin Company, for the United States Department of Energy's
National Nuclear Security Administration under Contract DE-AC04-94AL85000.

Issued by Sandia National Laboratories, operated for the United States Department of Energy by Sandia Corporation.

Available to DOE and DOE contractors from
U.S. Department of Energy
Office of Scientific and Technical Information
P.O. Box 62
Oak Ridge, TN 37831

Telephone: (865) 576-8401
Facsimile: (865) 576-5728
E-Mail: reports@adonis.osti.gov
Online ordering: http://www.osti.gov/bridge

Available to the public from
U.S. Department of Commerce
National Technical Information Service
5285 Port Royal Rd.
Springfield, VA 22161

Telephone: (800) 553-6847
Facsimile: (703) 605-6900
E-Mail: orders@ntis.fedworld.gov
Online order: http://www.ntis.gov/help/ordermethods.asp?loc=7-4-0#online

SAND2006-3494
Unlimited Release
Printed June 2006

Validation Experiments to Determine Radiation Partitioning of Heat Flux to an Object in a Fully Turbulent Fire

Allen Ricks, Thomas Blanchat, and Dann Jernigan
Fire Science and Technology
Department Names
Sandia National Laboratories
P.O. Box 5800
Albuquerque, New Mexico 87185-1914

Abstract

It is necessary to improve understanding and develop validation data of the heat flux incident to an object located within the fire plume for the validation of SIERRA/FUEGO/SYRINX fire and SIERRA/CALORE. One key aspect of the validation data sets is the determination of the relative contribution of the radiative and convective heat fluxes. To meet this objective, a cylindrical calorimeter with sufficient instrumentation to measure total and radiative heat flux had been designed and fabricated. This calorimeter will be tested both in the controlled radiative environment of the Penlight facility and in a fire environment in the FLAME/Radiant Heat (FRH) facility.

Validation experiments are specifically designed for direct comparison with the computational predictions. Making meaningful comparisons between the computational and experimental results requires careful characterization and control of the experimental features or parameters used as inputs into the computational model. Validation experiments must be designed to capture the essential physical phenomena, including all relevant initial and boundary conditions. A significant question of interest to modeling heat flux incident to an object in or near a fire is the contribution of the radiation and convection modes of heat transfer. The series of experiments documented in this test plan is designed to provide data on the radiation partitioning, defined as the fraction of the total heat flux that is due to radiation.

CONTENTS

1. Experiment Objective 9
   - 1.1 Background 9
   - 1.2 Guiding Principles for Validation Experiments 9
   - 1.3 Goals of the Present Experiments 11

2. Facility and Equipment 13
   - 2.1 Penlight 13
     - 2.1.1 Convective Flow Velocity Measurements in Penlight 16
     - 2.1.2 Convective Flow Temperature Measurements in Penlight 16
   - 2.2 FLAME/Radiant Heat (FRH) 19
     - 2.2.1 The FRH Test Cell 20
     - 2.2.2 Pre-test Simulations for Validation Experiment 21
     - 2.2.3 Convective Flow Velocity Measurements in FRH 22
     - 2.2.4 Convective Flow Temperature Measurements in FRH 23
   - 2.3 Cylindrical Calorimeter 24
     - 2.3.1 Structural Design 24
     - 2.3.2 Instrumentation 25

3. Design of experiments, testing procedures 28
   - 3.1 Design of Experiments 28
   - 3.2 Test Procedures 29

4. Data Acquisition and validation 30
   - 4.1 Data Acquisition 30
   - 4.2 Data Validation 30

5. Measurement Uncertainty 31
   - 5.1 Thermocouple Measurements 31
     - 5.1.1 Uncertainty of Overall System Excluding Mounting Errors 31
     - 5.1.2 Calorimeter Temperatures 33
     - 5.1.3 Penlight Convective Flow Temperature Measurements 34
   - 5.2 CARS Convective Flow Temperature Measurements 35
   - 5.3 Convective Flow Velocity Measurements 35
     - 5.3.1 Velocities in FRH 35
     - 5.3.2 Velocities in Penlight 35
   - 5.4 Heat Flux Measurements 36
     - 5.4.1 Medtherm HFGs 36
     - 5.4.2 Heat Flux Measurements made by Beck Engineering IHCP1D 38
     - 5.4.3 Convective Heat Flux Measurements 38
   - 5.5 Fuel Regression Measurements 38
   - 5.6 Measurement Uncertainty Summary 39

6. References 41

FIGURES

Figure 2-1. Thermocouple locations on the Penlight shroud (unrolled)..... 14
Figure 2-2. Heated back and side views of Penlight (with shroud extension). 15
Figure 2-3. Side, back, and front views of the cylindrical calorimeter in Penlight. 15
Figure 2-4. The annular gap between the cylindrical calorimeter and the Penlight shroud, as seen from the back end of Penlight..... 16
Figure 2-5. A cutaway view of the FRH facility showing a pool fire at the ground level, pipes supplying air flow through the basement, the chimney, and instrumentation rooms outside the FRH chamber..... 20
Figure 2-6. Measured mean velocities at the air ring in the basement of FRH (left) and at the ground level (right) [Ricks, 2006]. 21
Figure 2-7. Results of pre-test simulations showing expected size and temperature of fire, the free-stream gas temperature around the calorimeter, and heat fluxes to the calorimeter [Brown, 2006]..... 22
Figure 2-8. Basic schematic of the setup for PIV in FRH 23
Figure 2-9. Schematic of the basic cylindrical calorimeter assembly. 24
Figure 2-10. Insulation and plumbing in the cylindrical calorimeter. 25
Figure 2-11. TCs mounted to the inner surface of the calorimeter outer shell, HFG locations visible at four locations at the midplane. 26
Figure 2-12. Locations of TCs (black diamonds) and HFGs (open circles) on the outer shell of the cylindrical calorimeter (unrolled view)..... 27
Figure 5-1. Schematic of a Typical TC Data Acquisition System..... 31

TABLES

Table 2-1. Constants for Heat Transfer Correlation of Eq. (2.2). 18
Table 3-1. Cylindrical Calorimeter Radiation Partitioning Test Matrix 28
Table 5-1. Overall DAS Measurement Uncertainty Components..... 32
Table 5-2. Estimated Error in TC Readings in Air at 100ºC with a Velocity of 0.5 m/s. 34
Table 5-3. Uncertainties in Convective Heat Flux. 38
Table 5-4. Measurement Uncertainty Summary. 39

NOMENCLATURE

ASC	Advanced Strategic Computing
CARS	Coherent Anti-Stokes Raman Scattering
DAQ	Data Acquisition
DAS	Data Acquisition System
FLAME	Fire Laboratory for Accreditation of Models and Experiments
FRH	FLAME/Radiant Heat facility
HFG	Heat Flux Gauge
HP	Hewlett Packard
ID	Inner Diameter
LCBS	Lurance Canyon Burn Site
M&S	Modeling and Simulation
MIMS	Mineral-Insulated Metal-Sheathed
MUX	Multiplexer Units
NI	National Instrument
NIST	National Institute of Standards and Technology
OD	Outer Diameter
PIV	Particle Image Velocimetry
PSL	Primary Standards Laboratory
RHF	Radiant Heat Facility
RSS	Root-Sum-Square
SNL	Sandia National Laboratories
TC	Thermocouple
TTC	Thermal Test Complex
UPS	Uninterruptible Power Supply
V&V	Verification and Validation
WSEATC	Weapons Systems Engineering Assessment Technology Campaign

1. EXPERIMENT OBJECTIVE

1.1 Background

The cylinder is one of the canonical geometries for heat transfer, and is a relevant geometry to study the heat flux incident to an object located within the fire plume for the validation of SIERRA/FUEGO/SYRINX fire and SIERRA/CALORE thermal response codes. In particular, understanding the relative contributions of convective and radiative heat fluxes to an object in or near a fire is valuable for assessment of the interactions among FUEGO/SYRINX/CALORE during validation tests. To meet this objective, a cylindrical calorimeter with sufficient instrumentation to allow measurement of radiative and total heat fluxes has been designed and fabricated. This calorimeter will be qualified in a controlled, strongly radiating environment in the Penlight facility, following which a validation test in a fire environment will be performed in the FLAME/Radiant Heat (FRH) facility.

The cylindrical calorimeter was designed to enable validation of the coupling between FUEGO/SYRINX/CALORE. Data taken during each test will include measurements of the incident total heat flux to the object, the incident radiative flux to the object, the temperatures and velocities of the convective flow around the object, and the thermal response of the cylindrical object in a fully turbulent fire.

The goal of this report is to present the data validation steps and processes, as well as the test plan for the Penlight and FRH experiments that will be used to measure the total and radiative heat fluxes to the cylindrical calorimeter. This work complements the experimental studies done with the complex calorimeter [Blanchat et al., 2005], which emphasized the thermal response of a complex object in a fully turbulent fire, the complex calorimeter being used to validate the coupling of the fire field code (FUEGO) and the thermal response code (CALORE).

1.2 Guiding Principles for Validation Experiments

The discussion in this section follows the discussion in Blanchat, et al. [2005] and is discussed in greater depth in that reference.

The Weapons Systems Engineering Assessment Technology Campaign (WSEATC, also known as Campaign 6 or C6) is working with the Advanced Strategic Computing (ASC) program to change the way weapon components are designed and qualified. These changes complement an environment with limited testing and the requirements of stockpile stewardship. The amount of testing that can be done is limited by practical considerations such as small sample sizes and the inability to cover the entire environmental parameter space of interest.

One component of Campaign 6 provides the experimental capabilities and data required to validate the mathematical and computational models for the next generation of computational tools. Modeling and simulation (M&S) is the cornerstone of the strategy to balance the objectives of stockpile stewardship against the budgetary and time constraints of producing and qualifying hardware. Vigorous validation is an essential underpinning of confidence in the utilization of M&S tools. One of the major categories of validation experiments under Campaign 6 is the

characterization of abnormal thermal environments to which weapon systems may reasonably be subjected. The overall objective of this activity is to provide data to validate the field fire models of the FUEGO/SYRINX codes developed under the ASC applications program.

Validation experiments are a special class of experiment in that they are specifically designed for direct comparison with computational predictions. Making meaningful comparisons between the computational and experimental results requires careful characterization and control of the experimental features or parameters used as inputs into the computational model. Validation experiments must be designed to capture the essential physical phenomena, including all relevant initial and boundary conditions.

General Concepts for Experimental Validation of ASCI Code Applications [Trucano et al., 2002] defines and analyzes a process methodology that can be used in planning, executing, and assessing experimental validation projects and provides guidance as to what the ASC verification and validation (V&V) program believes are the correct characteristics of validation experiments. Characteristics are as follows:

1. Joint design of validation experiments from cradle to grave by analysts and experimentalists

2. Experiments aligned with the Phenomena Identification and Ranking Table of the Defense Program driver

3. Emphasize integration between experiment and calculation (nobody "throws information over the wall" to anybody else)

4. Emphasize scoping calculations to understand phenomena and help design instrumentation

5. Characterize experimental uncertainties sufficiently – diagnostic uncertainty, experiment variability – before performing experiments

6. Repeat experiments where possible

7. Properly identify and locate the role of model calibration in the validation activity, and define its impact on the validation activity

8. Quantitatively characterize ALL inputs needed for quantitative alignment of experiment and calculation

9. Use controlled experimental variability

10. Use different experimental facilities where possible

11. Perform redundant measurements on each experiment

12. Perform multiple measurements on each experiment

13. Use statistical design of experiments

14. Use statistical analysis of experiments

15. Exploit symmetry for redundancy and multiplicity

16. Document everything

1.3 Goals of the Present Experiments

The series of tests described in the present report have the following primary objectives:

1. Measure the radiative fraction of the incident heat flux in two scenarios, one dominated by radiative heat transfer from a hot object and another typical of a fire environment

2. Provide validation-quality data for modelers and code developers

The two types of experimental conditions given in the first objective are of fundamental interest for heat transfer studies and are commonly used in "abnormal thermal environments" experiments at Sandia National Laboratories. The results of the present series of tests will improve the understanding of heat fluxes in other experiments performed under similar conditions.

The second objective is to obtain data of sufficient quality that it will be useful for validating the simulation codes. The importance of validation was discussed in the preceding section. For validation data to be truly useful, it must be obtained to within an uncertainty bound that is comparable to or smaller than the computational uncertainty. Computational uncertainties are sometimes difficult to quantify, but some guidance can be obtained by performing sensitivity studies on model parameters, inputs, and boundary conditions. It is believed [Tieszen, 2006] that uncertainty in the total heat flux of the computational results is typically about ±30% but that errors as large as ±100% may occur. This is believed to be true over a range of heat fluxes ranging from approximately 40 kW/m^2 to 400 kW/m^2. Errors in the radiative and convective components of heat flux are expected to be similar to the total heat flux errors. The radiative fraction observed in typical sooting flames is approximately 0.8, but this fraction is much smaller for lightly sooting flames such as hydrogen or methanol.

To meet these objectives, the present set of experiments has the following set of goals:

1. Measure the total incident heat flux at the midplane of the calorimeter to ±35%

2. Measure the incident radiative heat flux at the midplane of the calorimeter to ±20%

3. Measure temperatures and velocities in the convective flow field to provide supplemental data for understanding the convective component of heat transfer

    a. Obtain temperature data to ±10%

    b. Obtain velocity data to ±15%

    c. Determine the convective heat flux from these temperature and velocity measurements to within ±50%

4. determine the radiative and convective fractions F_{rad} and F_{conv} (defined below) to ±0.10 (note that this is not a percentage but a fraction of the total heat flux)

In the present report, F_{rad} and F_{conv} will be defined as follows (Eq. (1.1)), where the subscripts *rad*, *conv*, and *total* refer to radiative, convective, and total heat transfer, respectively, and Q denotes the incident heat flux.

$$F_{rad} = \frac{Q_{rad}}{Q_{total}} \quad , \quad F_{conv} = \frac{Q_{conv}}{Q_{total}} \tag{1.1}$$

The determination of the fraction of the heat flux that is due to radiation (sometimes referred to as radiation partitioning of the total heat flux measurement) has been reported in the literature by Bryant, et al. [2003], Robertson and Ohlemiller [1995], and Wetterlund and Persson [1999], with measurement uncertainties estimated between 7 and 25% under the conditions of the experiments. Uncertainties are application-dependent.

2. FACILITY AND EQUIPMENT

2.1 Penlight

The cylindrical calorimeter is to be qualified in the Penlight apparatus prior to the fire experiments in FRH. The Penlight apparatus is a heated cylindrical cavity, 20.5 in. (520 mm) outer diameter (OD) and 32 in. (810 mm) long. The Penlight shroud is heated on the cylindrical sides by many quartz lamps. The shroud is fabricated from 1/8-inch thick rolled inconel (alloy 600). All interior surfaces are painted with a high-temperature black paint (Pyromark 2500, emissivity = 0.85 ± 0.09; see Nakos et al. [2004]). Twenty-eight thermocouples (TCs) are attached to the inner surface of the cylindrical shroud. Data from these TCs are logged on a Data Acquisition System (DAS) during tests. Seven thermocouples (1/16 in. or 1.6 mm diameter) are placed on each of the four axes, top (0°), right side (90°), bottom (180°), and left side (270°). Figure 2-1 gives the location of all TCs on the Penlight shroud. Note that additional TCs are used to control the power to the lamps (C) and to provide over-temperature protection (OT).

Back and side views of Penlight during a previous test are shown in Figure 2-3. The lamp array seen at the back end of Penlight will not be used for the cylindrical calorimeter tests. For the Penlight testing, the cylindrical calorimeter will be mounted coaxially inside the cylindrical Penlight shroud (Figure 2-3). Although the total length of the cylindrical calorimeter is much longer than the Penlight cavity, the instrumentation is concentrated close to the midpoint of the cylinder and will be within the Penlight cavity. The inner diameter (ID) of the Penlight cavity is approximately eight inches (20 cm) larger than the outer diameter (OD) of the cylindrical calorimeter, leaving an annular gap around the cylindrical calorimeter.

For the majority of the Penlight tests, the annular gap at both ends of the Penlight facility will be closed off with an insulating material (Durablanket, three layers of 1 in. (25 mm) thick blanket insulation material; see the front views of Figure 2-3). It is expected that this enclosure will minimize convective cooling by restricting the flow of cool air into the annular enclosure. In addition, the radiation emission field is expected to be more uniform in this configuration than with the ends open. Some tests will also be performed without the insulation endcaps. It is expected that natural convection will draw cool air from the surroundings through the annulus around the calorimeter. Differential pressure gauges and TCs will be used to measure the velocity and temperature of the air flowing past the calorimeter to provide further information on the convective heat fluxes.

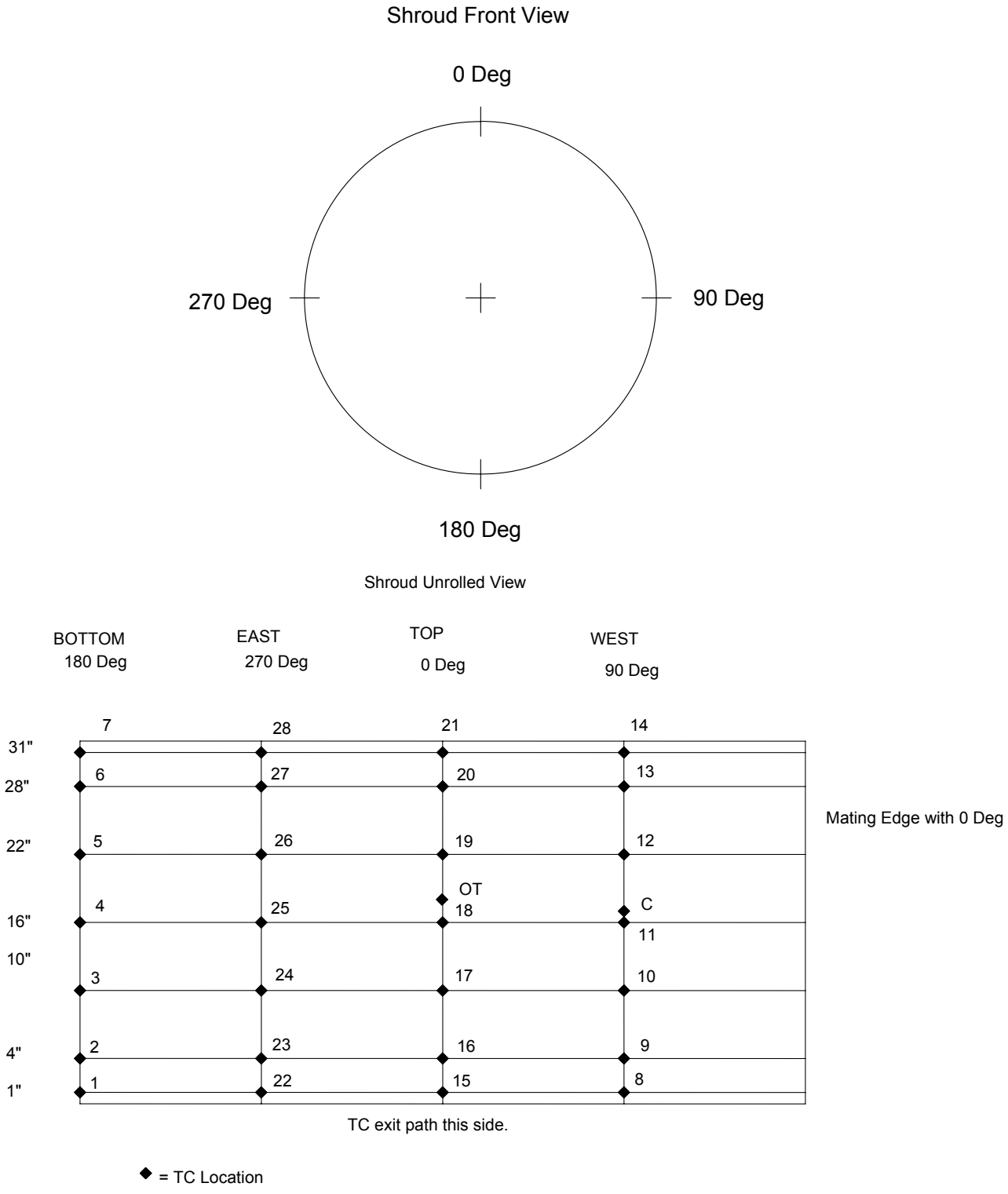

Figure 2-1. Thermocouple locations on the Penlight shroud (unrolled). TCs “OT” and “C” are inputs to the control system for over-temperature protection and for control of the heating lamps, respectively.

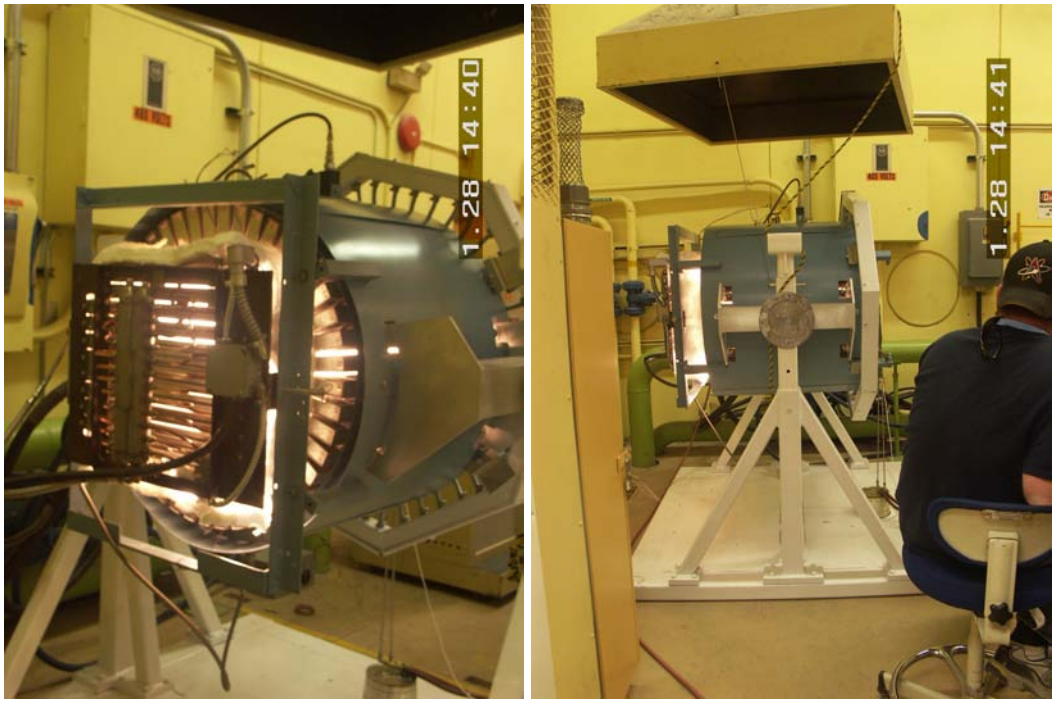

Figure 2-2. Heated back and side views of Penlight (with shroud extension).

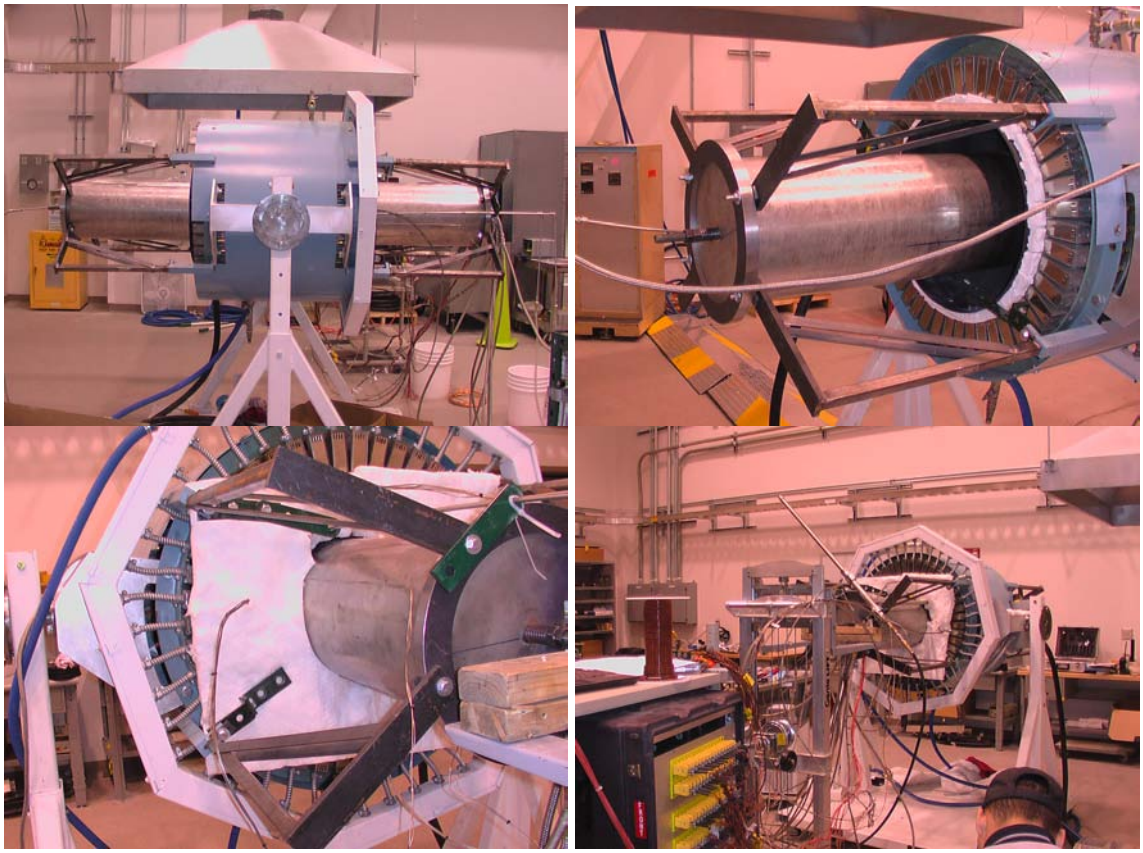

Figure 2-3. Side, back, and front views of the cylindrical calorimeter in Penlight.

2.1.1 Convective Flow Velocity Measurements in Penlight

For the test cases in the vertical orientation, the velocity of the airflow through the annulus between the cylindrical calorimeter and the Penlight shroud will be measured using a differential pressure probe designed for use in large pool fires [Kent and Schneider, 1987]. The probe is capable of withstanding elevated temperatures and is relatively insensitive to changes in flow direction. Pressure differences will be detected by a pressure transducer (Setra Model 264 very low differential pressure transducer) with a range of 0 – 0.05 in. WC (0 – 12 Pa) and recorded on a DAS.

For the test cases in which velocity data is desired, the probe is mounted approximately at the midpoint of the annular gap between the cylindrical calorimeter and the shroud, at approximately 315º in the coordinate system of the Penlight shroud (Figure 2-4, refer also to Figure 2-1), corresponding to an angular location at the midpoint between two of the heat flux gauges (HFGs). The differential pressure probe will be removed from Penlight during the tests in the horizontal orientation to reduce asymmetries or disturbances to the experimental conditions.

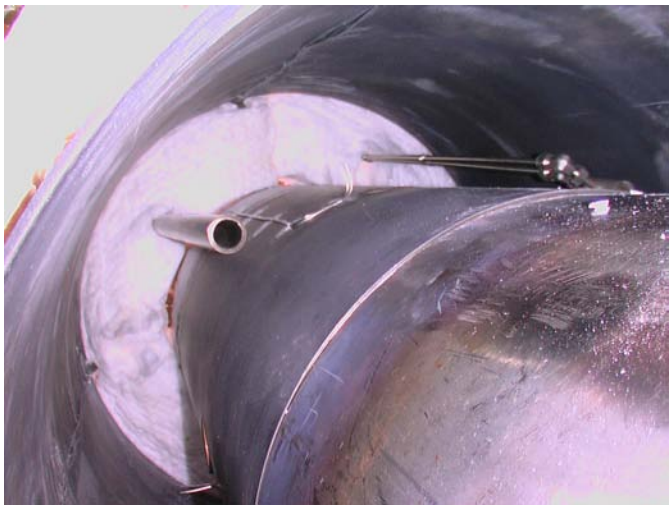

Figure 2-4. The annular gap between the cylindrical calorimeter and the Penlight shroud, as seen from the back end of Penlight. The shield surrounding the aspirated TC can be seen at the left and the differential pressure probe can be seen at the right of this picture.

2.1.2 Convective Flow Temperature Measurements in Penlight

Temperatures of the air flow past the cylindrical calorimeter in Penlight will be measured by an aspirated TC and/or two TCs of different sizes. TC readings of gas temperatures in strongly radiating flows may be subject to considerable errors and uncertainty due to the radiative heat transfer [Pitts et al., 1999]. Aspirated TCs are a proven method of reducing radiation errors but introduce significant disturbances to the flow field. A two-TC methodology for reducing radiation errors has been proposed by Brohez et al. [2004] but remains unproven. The Penlight tests of this report will apply the two-TC methodology and/or an aspirated TC, which will have the secondary benefit of providing an opportunity to evaluate the usefulness of the two-TC technique in practical applications.

2.1.2.1 Aspirated TCs

Aspirated TCs (also called suction pyrometers) minimize the errors due to radiation by shielding the TC from the radiation and drawing air past the TC at a velocity high enough to ensure that convective heat transfer dominates all other modes. The errors due to radiation tend to decrease as the suction velocity increases, but the errors due to temporal and spatial averaging, as well as perturbations to the overall flow field, will increase as the suction velocity is increased (see discussion in Pitts et al. [1999]). These disturbances may be significant in a natural-convection flow field such as that expected in Penlight.

The aspirated TC is a 20 mil (0.02 in. or 0.5 mm) mineral-insulated metal-sheathed (MIMS) TC at the centerline of a 1 in. (25 mm) OD stainless steel pipe which serves as a radiation shield and channel for the aspiration air flow. The TC is mounted 6 in. (150 mm) from one end of the pipe, which is positioned approximately 14 ¾ in. (0.375 m) from the back end of Penlight at an angular location of 45º in the Penlight coordinate system (Figure 2-4, refer also to Figure 2-1). The distance between the outer edges of the cylindrical calorimeter and the pipe is 5/8 in. (16 mm). The opposite end of the pipe extends out of the Penlight annulus and is connected to an air ejector (custom built by Fox Venturi Products, Fox Valve Development Corp.). Pressurized shop air regulated to 5 psi (35 kPa) gauge pressure is passed through a Venturi nozzle in the air ejector, creating suction on the pipe that serves as the shield around the aspirated TC. This draws air through the pipe and past the TC in the pipe, increasing the convective component of heat transfer to reduce the difference between the TC temperature and the air temperature.

The suction of the aspirated TC system in this application will remove a volume of air from Penlight when in use. The insulation over the ends of the Penlight cavity is porous enough that air from the room is then drawn into the cavity through the insulation. The addition of cooler air to Penlight, along with the change in the flow velocities in the cavity, may complicate the interpretation of the convective flow measurements when the aspirated TC is used in this application.

2.1.2.2 Radiation Correction for Two TCs of Different Sizes

An alternative approach has been demonstrated which attempts to reduce the error associated with bare bead TC measurements through the use of two TCs having different bead diameters but made from the same materials. By using two TCs of different sizes, an estimate of the radiation error can be obtained and thus a means of extrapolating the temperature back to what would be measured by a hypothetical TC that was not subject to radiation errors [Brohez et al., 2004]. This technique was not recommended by Pitts et al. [1999] for use in fluctuating temperature or radiation fields due to the finite time response of the TCs. The radiation fields in Penlight, however, will vary only slowly during most of the test cycle. As this technique is still relatively unproven, the Penlight tests offer an opportunity to evaluate the feasibility of the technique. If successful, the technique offers a means to correct for radiation errors, and the governing principles may help to bound the uncertainty in the measurements even if the radiation correction technique cannot be directly applied.

Following the methodology of Brohez et al. [2004], the radiation correction factor for the two-TC system is derived as follows. A simple steady-state energy balance for the TC, attributable to Blevins and Pitts [1999], can be written as in Eq. (2.1). The subscripts g, b, and ∞ refer to the gas, the TC bead, and the effective surrounding radiation temperature, respectively.

$$h\left(T_g - T_b\right) = \varepsilon_b \sigma \left(T_b^4 - T_\infty^4\right) \tag{2.1}$$

The convection heat transfer coefficient h is evaluated from an appropriate empirical correlation. Brohez et al. [2004] utilized a correlation for spheres appropriate for bare bead TCs. For the present work, the MIMS TCs can be approximated as isothermal cylinders in cross flow. Selecting for its simplicity a correlation attributed to Zhukauskas [1972] recommended by Incropera and DeWitt [1996], the convection heat transfer coefficient for the MIMS TCs is given in Eq. (2.2). All properties are evaluated at the gas temperature outside the boundary layer except for Pr_s, which is evaluated at the surface temperature of the TC. This correlation is appropriate for $0.7 < \mathrm{Pr} < 500$ and $1 < \mathrm{Re}_D < 10^6$, which is always satisfied for the present experiments at convection velocities greater than 32 cm/s. The exponent n is 0.37 if $\mathrm{Pr} \leq 10$ and is 0.36 if $\mathrm{Pr} > 10$. Other constants in Eq. (2.2) are given in Table 2-1.

$$h = \frac{k\,Nu_D}{D} = \frac{k}{D} C\,\mathrm{Re}_D^m\,\mathrm{Pr}^n \left(\frac{\mathrm{Pr}}{\mathrm{Pr}_s}\right)^{0.25} \tag{2.2}$$

Table 2-1. Constants for Heat Transfer Correlation of Eq. (2.2).

Re_D	C	m
1 – 40	0.75	0.4
40 – 1000	0.51	0.5

The Prandtl number of air is nearly constant over the temperature range $273\mathrm{K} \leq T \leq 2200\mathrm{K}$, so the ratio of Pr to Pr_s may be neglected for the present application. The ratio between the convection coefficients for the larger and smaller TCs in the same environment is given in Eq. (2.3), where it is assumed that both TCs are in the same Reynolds number range in Table 2-1. The subscript numbers distinguish between the two TCs. Since m is always less than one, Eq. (2.3) states that the convection coefficient of the smaller TC will be larger than that of the larger TC. This will increase the contribution of convection heat transfer, so the balance of Eq. (2.1) suggests that the smaller TC will in fact be less affected by radiation errors than the larger TC. It is this difference in convection coefficients upon which the theory for deriving a correction factor is built.

$$\frac{h_1}{h_2} = \left(\frac{D_1}{D_2}\right)^{m-1} \tag{2.3}$$

The correction factor can be expressed as in Eq. (2.4) in terms of an unknown effective surrounding temperature and the ratio of convection coefficients. This correction factor may be applied if the effective surrounding temperature can be estimated or measured. However, Eq. (2.4) may be subject to large errors if the denominator of the correction factor is near zero (i.e. the parameter α is close to unity).

$$\frac{T_g - T_1}{T_2 - T_1} = \frac{1}{1-\alpha} \quad , \quad \alpha = \frac{h_1 \varepsilon_2 \left(T_2^4 - T_\infty^4\right)}{h_2 \varepsilon_1 \left(T_1^4 - T_\infty^4\right)} \tag{2.4}$$

The expression (Eq. (2.5)) developed by Brohez [2004] can be derived from Eq. (2.4) using the steady-state balance of Eq. (2.1) to solve for the effective radiation temperature. As compared to Eq. (2.4), this expression is less sensitive to division-by-zero errors (see Eq. (2.3)) but requires greater knowledge of the convection coefficients which depend upon the unknown gas temperature and velocity. The gas temperature can be solved iteratively, but if the velocity is not measured in the region of the TCs then it must be modeled in some fashion. Velocities at the TCs, are not measured in the Penlight tests, and the determination of the convection coefficients for the present study is therefore subject to large uncertainty.

$$\frac{T_g - T_1}{T_2 - T_1} = \frac{\varepsilon \sigma \left(T_2^2 - T_1^2\right)\left(T_2 + T_1\right)}{h_2 - h_1} + \frac{1}{h_2 - h_1} \tag{2.5}$$

Brohez et al. [2004] presented theoretical results showing the correction factor to be nearly constant over a wide range of quasi-steady flow conditions; however, the actual correction factor of their experiments was subject to very large variations. The experimental correction factor had a mean value close to that predicted by the theory, and they suggested that a typical value of the correction factor be used as a user-friendly tool to estimate the effects of radiation. Further analysis of the procedure under the conditions of the Penlight tests is required in order to evaluate the practicality of the technique and to determine whether Eq. (2.4), Eq. (2.5), or a constant correction factor is most suitable for this application.

For convenience and uniformity, the TCs for measuring the convective flow temperature in Penlight are mounted to the cylindrical calorimeter rather than to the Penlight shroud. MIMS TCs of 20 mils and 1/16 in. (0.5 and 1.6 mm) diameter are mounted 1 in. (22 mm) off the surface of the calorimeter at angular locations 0º, 90º, 180º, and 270º in the Penlight coordinate system. These angular locations correspond to the locations of HFGs on the calorimeter and were chosen to provide data on the temperature of the convective flow over the total HFGs. The TCs are mounted 3 in. (76 mm) and 3.5 in. (89 mm) from the midplane of Penlight, for the 1/16 in. and the 20 mil TCs, respectively, in the direction of the exit path of the TCs.

2.2 FLAME/Radiant Heat (FRH)

The cylindrical calorimeter will be tested in a fire environment in FRH. For these tests, the cylindrical calorimeter will be placed 1 m above a pool of methanol 2 m in diameter with enough methanol to burn for 5 – 15 minutes. The response of the cylindrical calorimeter in a fully engulfed fire scenario will be tested. Flow velocities outside the calorimeter will be studied using Particle Image Velocimetry (PIV), and the temperature of the convective flow will be measured with Coherent Anti-Stokes Raman Scattering (CARS).

2.2.1 The FRH Test Cell

The FRH test cell is part of the Thermal Test Complex (TTC) at Sandia National Laboratories (SNL). The main test chamber of the FRH cell is cylindrical in shape, 60 ft (18 m) inner diameter with a height around the perimeter of 40 ft (12 m). The ceiling slopes upwards (~18º) from the perimeter walls to a height of 48 ft (15 m) over the center of the facility. A round hole at the top of the facility 16 ft (4.9 m) diameter transitions to a 10 ft by 12 ft (3.0 m by 3.7 m) chimney duct (see Figure 2-3). The outer walls are made of steel channel sections and are filled with water for cooling during tests.

The ground level of FRH can be divided into three concentric sections. At the center of the facility is a fuel pan or gas burner. The facility can operate a 3 m diameter gas burner (He, H_2, CH_4, etc.) or a liquid fuel pool (JP8, methanol, etc.). The radiation partitioning tests will utilize a 2 m pool. The second section is a steel spill plate, which extends to a diameter of 6 m. The floor of the outer section is made of a steel grating, through which air is supplied to the FRH chamber during fire experiments. FRH is designed for flexibility in fuel types; for the present experiments methanol will be used as the fuel due to its low sooting propensity. The laser diagnostics used in the present experiments are difficult to perform in heavily sooting flames due to attenuation or interactions with the soot particles.

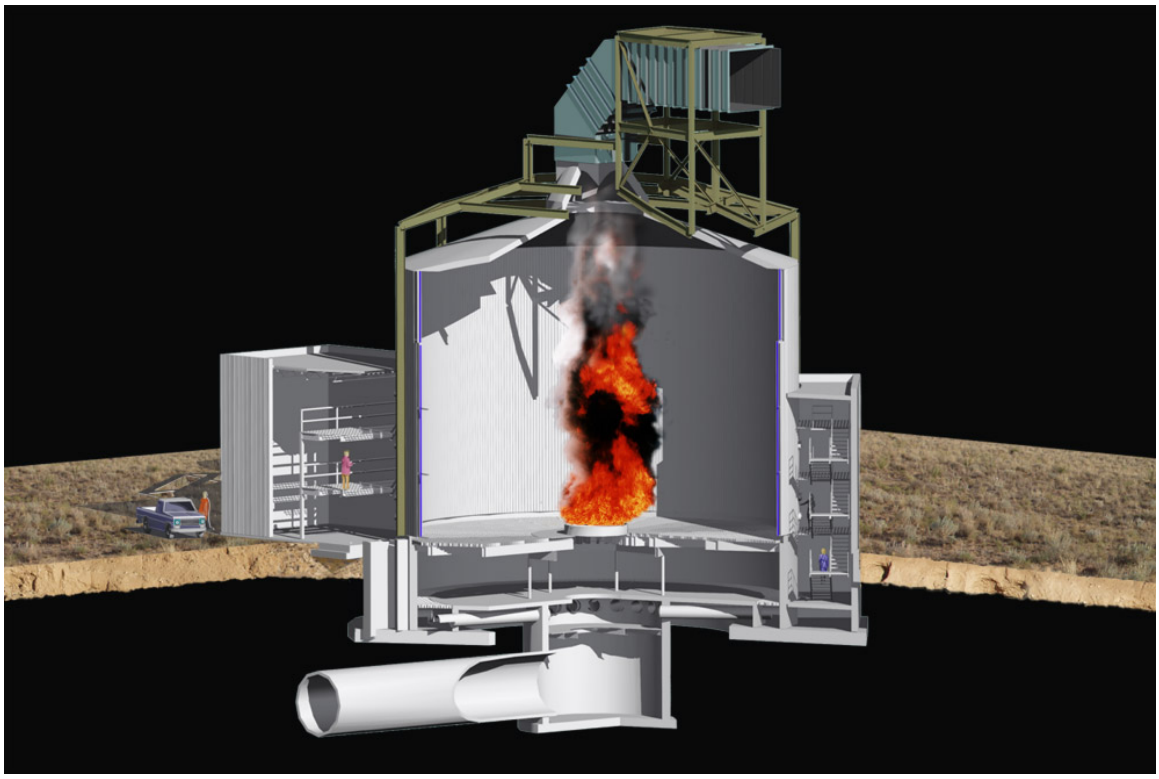

Figure 2-5. A cutaway view of the FRH facility showing a pool fire at the ground level, pipes supplying air flow through the basement, the chimney, and instrumentation rooms outside the FRH chamber.

The air flow in the FRH chamber combines contributions due to the buoyancy-controlled fire and due to the forced flow of air through the facility. The air flow in the absence of a fire has been characterized experimentally at the air ring in the basement and at the ground level [Ricks, 2006]. The air ring flow field was found to exhibit a pattern (left side of Figure 2-6) attributable to the 18 supply pipes carrying the air from the diffuser in the center of the facility to the air ring along the outer edges of the facility (refer to Figure 2-5). The air flow at the ground level was found to be highest in the outer portion of the FRH cell, and exhibited a large recirculation zone in the inner portion of the facility, where mean velocities were in the negative (downward) direction (right side of Figure 2-6). The presence of a fire at the center of the facility is likely to reduce the recirculation because the air flow will be drawn inwards and entrained into the buoyant fire plume.

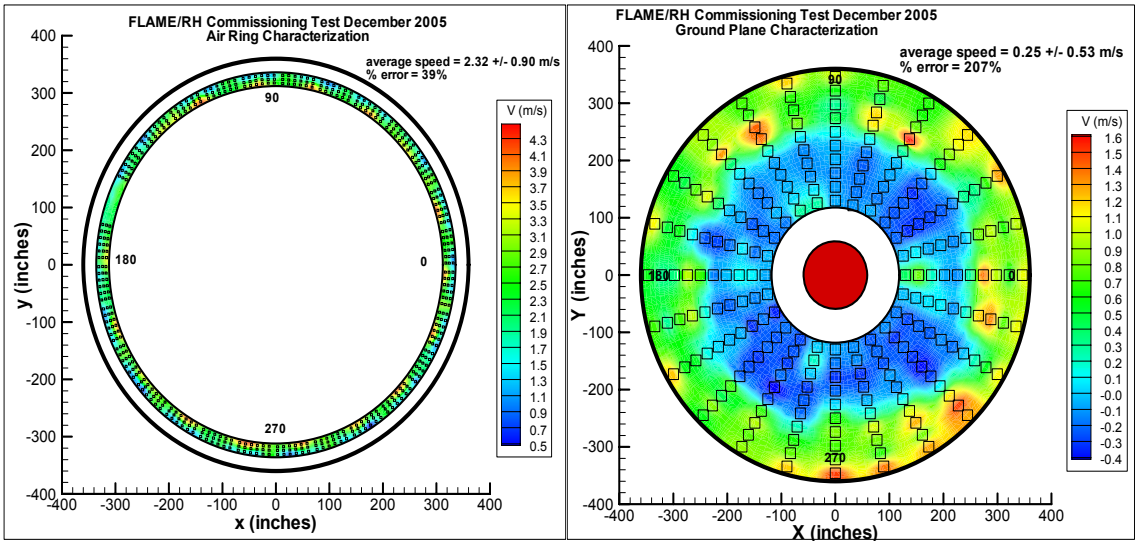

Figure 2-6. Measured mean velocities at the air ring in the basement of FRH (left) and at the ground level (right) [Ricks, 2006].

2.2.1.1 Fuel Regression Measurements

Burning rates for liquid pool fires are determined by the evaporation rate of the fuel. For the present test in FRH two Rosemount Model 3051 differential pressure gauges (0 – 25 in. WC) will measure the pressure difference between the ambient pressure and the pressure at the bottom of the pan. The evaporation rate of the fuel can be determined from the rate of change of pressure at the bottom of the pool and the fuel's specific gravity.

2.2.2 Pre-test Simulations for Validation Experiment

Pre-test simulations were carried out [Brown, 2006, reproduced in Appendix A of this report] to help guide the development of the experiments in FRH, in accordance with minimum guidelines for validation tests. The simulations were performed on two different computational grids, and results from the two simulations showed good general agreement. Only results from the finer grid are shown in the body of this report (Figure 2-7). The plots in Figure 2-7 are the averaged temperature, two instantaneous views of the 900 K isotemperature surface, the averaged free-stream gas temperature around the calorimeter, and the averaged convective and incident radia-

tive heat flux to the calorimeter. Predicted flame height is approximately 1.5 times the pool diameter, as based on the 900 K temperature surface. The simulation predicts that the ends of the calorimeter will not be engulfed in the fire and that the highest heat fluxes will not be located at the midplane of the calorimeter. Maximum values for the radiative heat flux were approximately 120 kW/m^2; maximum values for the convective heat flux were approximately 20 kW/m^2. For further details, see Appendix A.

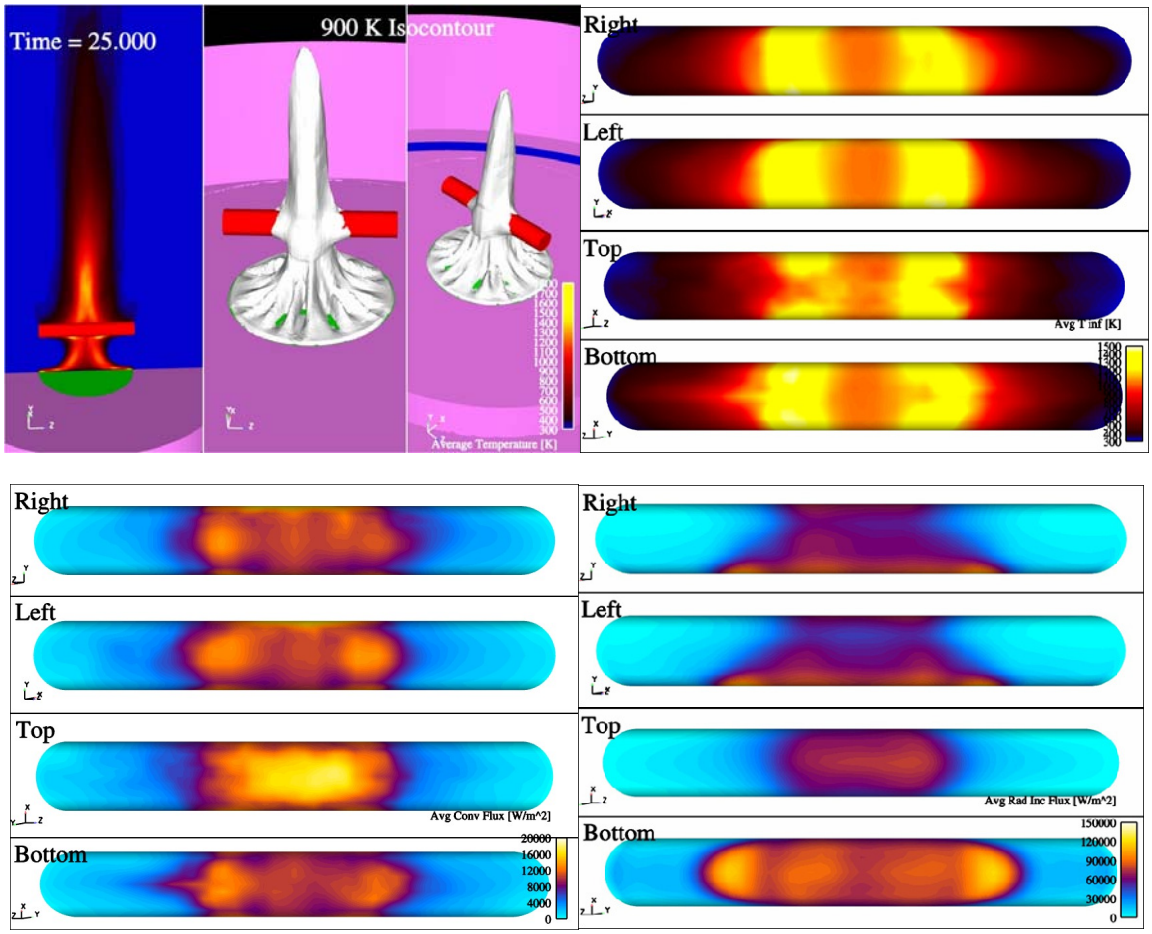

Figure 2-7. Results of pre-test simulations showing expected size and temperature of fire, the free-stream gas temperature around the calorimeter, and heat fluxes to the calorimeter [Brown, 2006].

2.2.3 Convective Flow Velocity Measurements in FRH

The PIV system used to measure velocities in a fire in the near field around the cylindrical calorimeter in FRH is shown in Figure 2-8. Two Coherent Infinity Q-switched Nd:YAG lasers will be used to generate a single collinear sheet with a pulse delay of 1-5 ms. The laser wavelength is 532 nm, and the energy output is 250 mJ per 8 ns pulse for each system at up to 100 Hz repetition rate. Image pairs will be digitally recorded on a Kodak ES-1 interline transfer CCD camera, with a 1 K × 1 K pixel format. The camera is capable of recording 15 image pairs per second with 6 μs to 30 ms delay between images. The camera will be synchronized with the lasers so that the laser pulses occur when the camera shutter is open. Flow field velocities will be meas-

ured by cross-correlation of particle locations between subsequent frames in an image pair, so 15 velocity maps per second will be produced. PIV has previously been applied for measurements in methanol pool fires, methane and hydrogen gas fires, and nonreacting helium plumes in previous SNL programs (e.g., Tieszen et al., 2002, 2004; O'Hern et al., 2005).

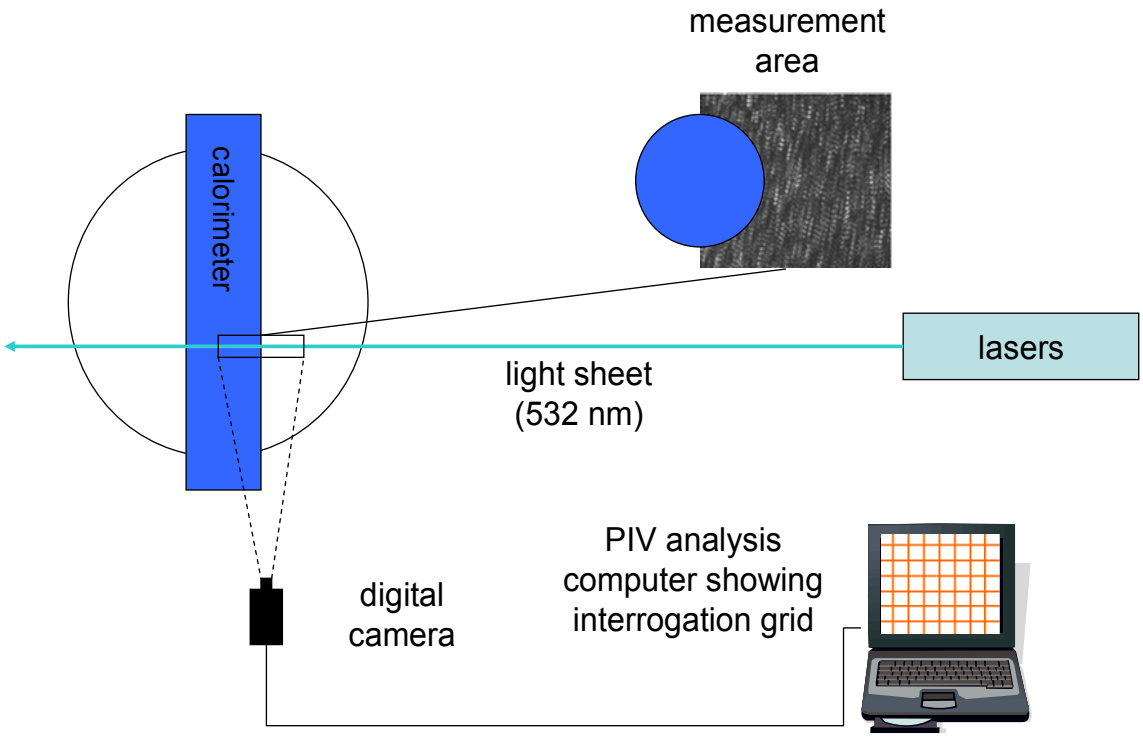

Figure 2-8. Basic schematic of the setup for PIV in FRH. The calorimeter will be oriented parallel to the camera axis to capture velocity field information around the cylindrical calorimeter body.

2.2.4 Convective Flow Temperature Measurements in FRH

Gas temperatures in the FRH experiments will be measured using CARS of the nitrogen molecule. CARS provides a point measurement of gas temperatures by a noninvasive, laser-based probing of the reacting flowfield. The details of the CARS process for probing sooting flames are provided by Kearney [2006]. Only a procedural summary the CARS measurements at FRH is provided here. Two pulsed laser beams are propagated into the FRH cell from the attached diagnostics laboratory. The laser beams are crossed at a common focus to form a CARS probe volume just outside of the thermal boundary layer of the cylindrical calorimeter. The difference in wavelength between the two beams is tuned to drive the rotational-vibrational Raman transitions of nitrogen and a laser-like CARS signal is generated within the CARS probe volume. The CARS signal beam is forward propagated to a high-resolution grating-based spectrograph and the CARS signal spectrum is captured using a CCD camera. The spectral content of the CARS signal reveals how nitrogen population within the CARS probe volume is distributed among the allowed rotational and vibrational states and the gas temperature is determined from a best fit of theory to the experimentally obtained spectra.

2.3 Cylindrical Calorimeter

2.3.1 Structural Design

The cylindrical calorimeter is comprised of a center section 18 in. (0.46 m) in length, within which all of the sensors are mounted, and two end sections of length 30 in. (0.76 m) each. All three sections are made of 1/8-in. stainless steel (alloy 304) and have an OD of 12 in. (0.30 m). The basic design of the calorimeter and its internal structure are shown in Figure 2-9. A 2-in. (50 mm) steel pipe down the center of the calorimeter forms the backbone of the structure, and the outer shells are held in place by four center supports in the shape of an eight-pointed star. Steel end caps 0.5 in.-(13 mm-) thick complete the structure of the calorimeter.

The entire inside of the calorimeter is filled with Fiberfrax brand insulation materials. Two types of insulation are used (see Figure 2-10). The center section is filled with a ceramic fiber blanket insulation (Durablanket S type, rated to 2300ºF (1260ºC), 8 lb/ft^3 density (128 kg/m^3)). The primary insulation used in the outer sections is a board type (Duraboard), with blanket insulation used to stuff the gaps where the board insulation could not be used. The outer surface of the center section of the cylindrical calorimeter is painted with Pyromark 2500 paint. The inner surface of the calorimeter, the cylindrical end sections, end caps, etc. are unpainted.

Heat flux measurements are obtained through two different measurement techniques, in accordance with the guiding principles of validation experiments presented in Section 1.2. The instrumentation and methodology will be discussed briefly in the following section.

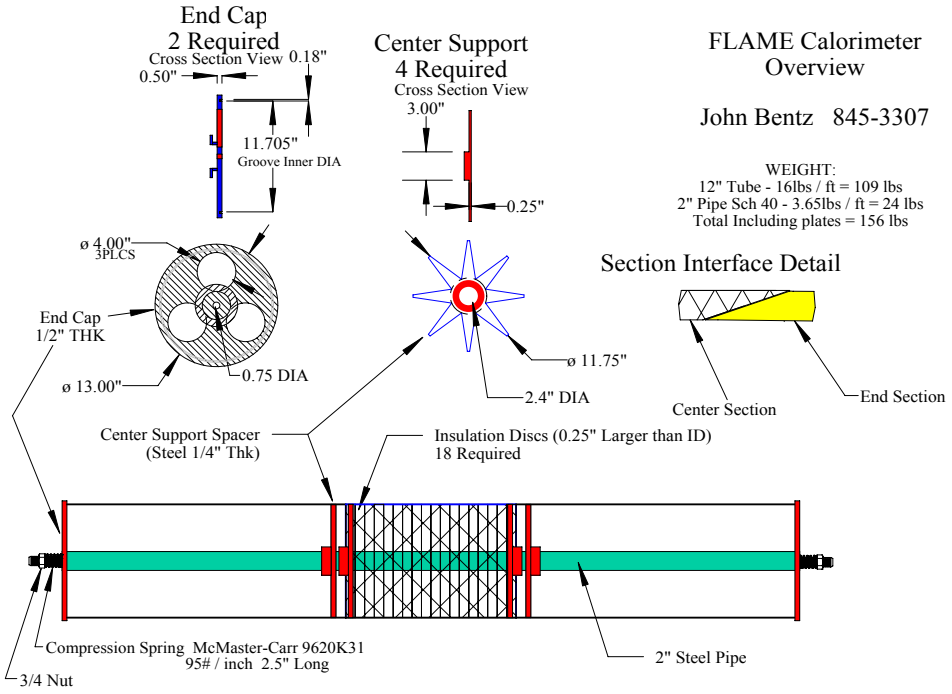

Figure 2-9. Schematic of the basic cylindrical calorimeter assembly.

Figure 2-10. Insulation and plumbing in the cylindrical calorimeter.

2.3.2 Instrumentation

2.3.2.1 Calorimeter TCs

A total of 36 TCs (40 mil (1.0 mm) MIMS type) are attached to the inside of the outer shell of the center section, located on a uniform 5 × 8 grid. The grid spacing in the axial direction is 3 in. (76 mm) between TC locations, and the angular spacing is 45º about the axis of the calorimeter. Four grid locations at the midpoint of the cylindrical calorimeter are occupied with heat flux gauges (HFGs) in place of TCs (see Figures 2-11 and 2-12 for TC and HFG locations on the cylindrical calorimeter).

The primary purpose of the TCs on the outer shell is to provide data on the heat flux. The net heat flux at each TC location can be estimated from the temperature history, material properties, and assumed boundary conditions using an inverse heat conduction methodology. The assumption of 1-D heat conduction is typically used and errors will increase if 2-D effects are significant [Lopez et al., 2000]. The 1-D assumption will be invoked in the present work because all of the calorimeter TCs are located in the center section of the calorimeter, far from the ends of the Penlight cavity, and the calorimeter is heated from all sides. For the present series of tests, the software used to estimate the heat flux from the temperature measurements is IHCP1D (commercially available through Beck Engineering).

Two TCs are mounted inside the calorimeter in addition to the 36 TCs mounted to the inner surface of the outer shell. One TC is mounted on the cooling water return line for one of the HFGs. The other is mounted in the center of the bundle of wires for the calorimeter TCs and HFGs, near the steel pipe at the axis of the calorimeter. These TCs monitor the health of the system and can be used as a check of the DAS, since the temperatures at these locations are expected to vary only slowly.

Figure 2-11. TCs mounted to the inner surface of the calorimeter outer shell, HFG locations visible at four locations at the midplane.

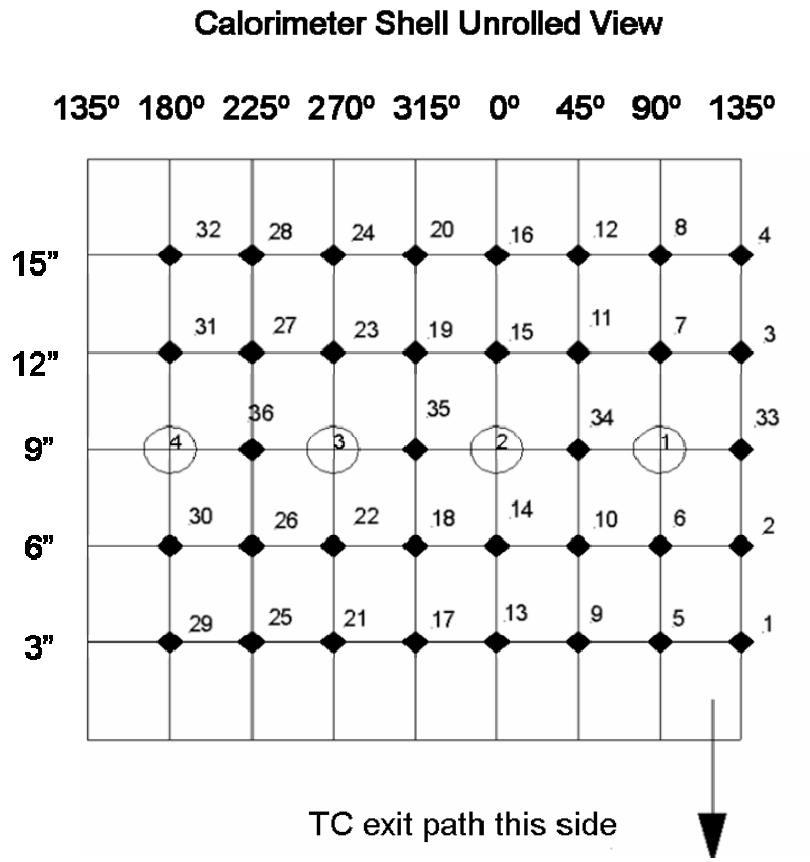

Figure 2-12. Locations of TCs (black diamonds) and HFGs (open circles) on the outer shell of the cylindrical calorimeter (unrolled view). Grid spacing in the axial direction is 3 in. (76 mm).

2.3.2.2 Heat flux gauges

The cylindrical calorimeter also contains four Medtherm (Model 96-15T-15RP(ZnSe)-21745) dual-mode HFGs at the midpoint of the calorimeter. The angular spacing between the gauges is 90º, at angular values 0º, 90º, 180º, and 270º in the coordinate system of the cylindrical calorimeter (refer to Figure 2-12). Each gauge contains both a total heat flux transducer with a 180º view angle and a gas purged radiometer with a 150º view angle. The combination of these two types of gauges allows direct measurement of the total and radiative heat fluxes, from which the convective heat flux may be inferred. Both are Schmidt-Boelter gauges, which use a thermopile to extract a heat flux from a small temperature difference on the front and back sides of a thin wafer of a thermally stable material. The body of the gauge is water cooled. The required lines and hoses for the water cooling and gas purging, along with electrical wiring for the TCs and HFGs, are routed inside the calorimeter to the calorimeter endplates (this can be seen in Figures 2-3 and 2-10).

Heat flux measurements may be sensitive to a variety of factors. In the Penlight experiments discussed in this report, the disturbances and possible error sources will be minimized by not using the nitrogen purge for the radiometers. The purge will be used in the fire tests in FRH, where the radiometer window might otherwise be clogged with soot.

3. DESIGN OF EXPERIMENTS, TESTING PROCEDURES

3.1 Design of Experiments

The C6 radiation partitioning experiments will be performed over a series of seven tests, as shown in Table 3-1. The tests will be performed both in Penlight, where the radiation environment can be carefully controlled, and in FRH, where the calorimeter can be subjected to radiative and convective heat fluxes resulting from actual fires.

Table 3-1. Cylindrical Calorimeter Radiation Partitioning Test Matrix

Test Facility	Calorimeter Orientation	Calorimeter Axis Location	Air Flow Around Calorimeter	Roll Angle
Penlight	Horizontal	Coaxial with Penlight	Restricted by insulation over ends of annulus	0º
Penlight	Horizontal	Coaxial, as above	Restricted, as above	90º
Penlight	Horizontal	Coaxial, as above	Restricted, as above	180º
Penlight	Horizontal	Coaxial, as above	Restricted, as above	270º
Penlight	Vertical	Coaxial, as above	Restricted, as above	N/A
Penlight	Vertical	Coaxial, as above	Unobstructed through Penlight annulus	N/A
FRH	Horizontal	Over center of pool	Unobstructed	0º

The first four Penlight experiments are designed to check the uniformity of the readings from each of the four Medtherm dual HFGs, as well as to provide data on heat fluxes to a horizontal cylinder in a controlled radiation environment. For all of these tests, the gap between the calorimeter and the Penlight apparatus will be covered with insulating material at the front and back ends of the Penlight shroud. By covering the ends with insulation, the amount of cool air that will be drawn into the calorimeter is restricted and the experiments will be less affected by convective heat transfer effects.

Two experiments will be performed in Penlight in the vertical orientation. This orientation is also of interest because in accident scenarios it is not always possible to predict the orientation of a weapon, and it may be expected that the heat flux to the calorimeter may differ due to differences in free convection effects. The free convection effects will be further studied by testing the vertical cylindrical calorimeter in Penlight under two boundary conditions. The first will be with the gap between the calorimeter and the Penlight shroud sealed at the top and bottom with insulating material, as described previously for the tests in the horizontal orientation. The second configuration differs in having the insulation removed, allowing unobstructed airflow through the annular gap between the calorimeter and the Penlight shroud. It is expected that this will increase the effect of the convective heat flux because cool room air may be freely drawn into the gap and alongside the calorimeter. Velocities and temperatures of the air flowing through the calorimeter-Penlight annulus will be measured to enable further analysis of the convective heat flux.

Finally, the cylindrical calorimeter will be tested in FRH to measure radiation and total heat transfer to the calorimeter in a fire situation. The calorimeter will be mounted 1 m above the pan, across the center of the pool. Gas temperatures and velocities in the near field around the calorimeter will be measured for analysis of the effects of convection.

3.2 Test Procedures

All Penlight tests will be performed in the following manner. Data logging for all of the instrumentation in Penlight and the cylindrical calorimeter will begin with the Penlight shroud and the calorimeter at approximately room temperature. After several minutes of data logging, the Penlight temperature controller will be set at 300ºC; the shroud typically reaches this temperature less than two minutes after the change in temperature is input to the controller. The Penlight shroud will be allowed to stabilize at this temperature and held there for at least ten minutes. The shroud temperature controller will then be set to 600ºC, again reaching the specified temperature approximately two minutes after the input is entered. After 10 to 15 minutes at this temperature, the shroud heating lamps will be turned off and the shroud and calorimeter will be allowed to cool naturally to ambient temperatures.

Tests in FRH will be performed with a methanol (CH_3OH) fire. Methanol burns with a blue flame and produces very little soot, which greatly simplifies the use of laser diagnostics techniques. In the radiation partitioning experiments, laser diagnostics will be used to measure the velocity (PIV) and the temperature (CARS) of the convective flow around the calorimeter. A 2 m fuel pan will be filled with enough fuel for a 5 to 15 minute burn. The calorimeter will be positioned in a horizontal orientation approximately 1 m above the surface of the pool. The access doors of the FRH chamber will be closed and the fans supplying the air flow will be turned on. Gas temperatures and velocities in the flow field near the calorimeter, and temperatures and heat fluxes measured by the calorimeter, will be recorded from shortly before pool ignition to burnout.

4. DATA ACQUISITION AND VALIDATION

4.1 Data Acquisition

The DAS consists of a PC with a 16-bit data acquisition card connected to a National Instruments (NI) SCXI-1001 chassis. It has 12 NI SCXI-1102 cards with NI SCXI-1303 blocks for TCs and four NI SCXI-1104 cards with NI SCXI-1300 blocks for analog signals. This provides the ability to increase either analog signals or TC signals. Note that the SCXI-1001 presently holds 12 cards, yielding a total channel count of 384 channels if all slots are used for data acquisition. The system is upgradeable simply by adding an additional SCXI-1001 DAQ card and more multiplexer units (MUXs).

The data acquisition system can acquire temperature, heat flux, and pressure data. The integrity of all TC channels is evaluated prior to each experiment with an Ectron TC, which inputs a controlled signal into each channel at the TC device connection point and provides a check on the integrity of the channel hardware and software from that point to the final magnetic storage location. The TC simulators are calibrated yearly in the SNL Standards Laboratory that ties back to a National Institute of Standards Technology (NIST) standard.

Data are sampled simultaneously for all channels, typically at 1000 Hz with an average value recorded at a rate of at least one sample per second, starting approximately two minutes ($\pm$ 2 minutes) prior to the start of a test and continuing after a test, if collection of cooldown data is desired.

A formal checklist for conducting the test is created and used to record actions during the test event. Test event data include both actions taken during the test (i.e., a completed checklist) and data gathered electronically from the instrumentation. The data from the instrumentation are organized via a Data Channel Summary Sheet and with sketches showing instrumentation location. This summary sheet contains a channel-by-channel listing of the instrumentation with details such as expected range, sampling rate, calibration date and source, instrument location, and the data sample rate. Post-test, all data are collected and converted to electronic format for purposes of archiving and dissemination via PC media (i.e., CD or equivalent).

4.2 Data Validation

All channels had an uncertainty to within $\pm$1.7 K (see Section 5, below). Data validity checks such as checking for TC shunting* and obvious failures were performed on all channels. Obvious faults (e.g., physically impossible values, non-readings, readings inconsistent with other similar readings) were used to eliminate faulty channels.

Additionally, each calorimeter TC was heated with a heat gun after attachment to ensure each channel was properly identified and to assess the homogeneity of the exposed portions of the TC.

* Shunting is a phenomenon that occurs when the magnesium oxide insulation inside the TC reaches a high enough temperature so that its electrical resistivity decreases significantly. When this occurs "virtual" junctions form so the TC shorts or "shunts" and incorrect readings occur.

5. MEASUREMENT UNCERTAINTY

5.1 Thermocouple Measurements

5.1.1 Uncertainty of Overall System Excluding Mounting Errors

In order to enhance scientific understanding or validate computer models, the uncertainty of the experimental data used for those purposes must be determined. The following summarizes the description and uncertainty estimates for TC DASs for SNL's experimental facilities that routinely gather data from normal and abnormal thermal environment experiments, specifically the Penlight apparatus and the FRH facility. In most respects, the systems and uncertainties are the same as for two of SNL's experimental facilities that have previously been used for the same purposes; the Radiant Heat Facility (RHF) and Lurance Canyon Burn Site (LCBS) [Nakos, 2004].

Figure 5-1 gives an example of a typical DAS used for thermal experimentation, separated into the following components:

1. TC;
2. TC connectors;
3. TC extension cable;
4. TC plug board;
5. National Instruments DAQ system;
6. Data reduction computer.

The uncertainty of the entire TC DAS was estimated by looking at the individual uncertainties of each component, then combining them using the root-sum-square (RSS) method [Coleman and Steele, 1999].

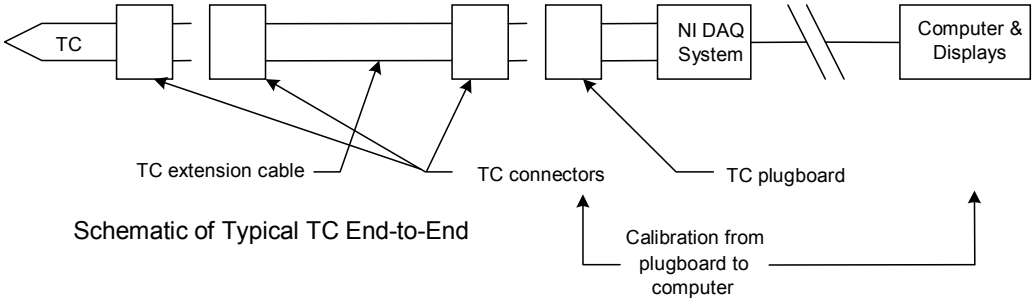

Figure 5-1. Schematic of a Typical TC Data Acquisition System.

Nakos [2004] performed uncertainty analyses for several TC data acquisition systems used at the RHF and LCBS. These analyses apply to Type K, chromel-alumel thermocouples in MIMS TC assemblies and other applications. Several DASs were analyzed: one Hewlett-Packard (HP) 3852A system, and several National Instrument (NI) systems. The uncertainty analyses were performed on the entire system from the TC to the DAS output file. Uncertainty sources include TC mounting errors, ANSI standard calibration uncertainty for Type K TC wire, potential errors due to temperature gradients inside connectors, extension wire effects, DAS hardware uncertainties including noise, common mode rejection ratio, digital voltmeter accuracy, mV to temperature conversion, analog to digital conversion, and other possible sources. Typical results for "normal" environments (e.g., maximum of 300-400K) showed the total uncertainty to be about ±1% of the reading in absolute temperature. In high-temperature or high heat-flux ("abnormal") thermal environments, total uncertainties range up to ±2–3% of the reading (maximum of 1300K). The higher uncertainties in abnormal thermal environments are caused by increased errors due to the effects of imperfect TC attachment to the test item. Any systematic bias errors that can be modeled, such as those due to TC attachment imperfection, are algebraically subtracted from the TC reading, and any modeling uncertainty about the nominal mean estimate of the bias is included in the RSS calculation [Romero et al., 2004; 2005].

Table 5-1 provides a summary of the uncertainty sources present in a typical TC measurement. In this table, B_T and S_T indicate the total systematic and random uncertainties, respectively. In effect, Table 5-1 quantifies the uncertainty of the measurement of the TC temperature; the actual desired temperature (of the calorimeter shell, Penlight shroud, or air in Penlight) is subject to additional bias errors due to mounting. These bias uncertainties are very hard to accurately quantify, are application dependent, and are often the largest errors in the measurement system.

Table 5-1. Overall DAS Measurement Uncertainty Components.

Component	Systematic Error or Uncertainty*	Random Uncertainty**	Source/Comments
1. Type K, chromel-alumel TC	From 0-277°C, uncertainty is ±2.2C; above 277°C uncertainty is ±0.75% of the reading in °C. At 1000°C this is ± 7.5°C	NA	ASTM Manual on Use of Thermocouples
2. TC connectors	±0.5°C due to possible temperature gradients across connector. Assume ± 0.5°C	NA	Uncertainty Analysis of TC Measurements
3. TC extender cable	±2.2°C from 0-204°C		ASTM Manual on Use of TCs
4. Plug board to computer: sources covered by Ectron calibration	Uncertainties assumed to be random even though some are random and some systematic	Maximum errors were about +1.7°C, -0.4°C at 100°C and +1.7°C, -0.6°C at 1000°C. Use ±1.7° C for simplicity	Calibration doesn't make distinction between systematic or random error. Uncertainty sources include nonlinearity, offset, gain error, scan speed, normal mode noise rejection (60 Hz)

Table 5-1. Overall DAS Measurement Uncertainty Components.

Component	Systematic Error or Uncertainty*	Random Uncertainty**	Source/Comments
5. Sources not covered by Ectron calibration	Filter cutoff: -3dB at 2 Hz: ignore Filter step response: to 0.1% = 1 sec At 100°C this is 0.1°C; at 1000°C this is 1.0°C. Long term stability = 20μV/°C for gain=1: 0.25°C Gain temperature coefficient = 10ppm/°C: 0.001% - negligible	e) Common mode rejection ratio for gain = 100 is ±1°C This assumes common mode voltage is equal to maximum TC output (-41mV)	Filter cut-off and step response, common mode rejection ratio, long term stability not covered by Ectron calibration
Total systematic and random uncertainties	$B_T = (\Sigma B_i^2)^{1/2}$ = ±5.3°C (1000°C) or ±2.2°C at 100°C	$S_T = (\Sigma S_i^2)^{1/2}$ = 0.66°C at either 100°C or 1000°C	Combine using RSS method, * and ** notes
Overall TC measurement uncertainty	$U_{95} = \pm 2[(B_T/2)^2 + S_T^2]^{1/2}$ $\pm 5.5\,°C$, *or* $\pm 0.4\%$ @ 1000 °C $= \pm 2.6\,°C$, *or* $\pm 0.7\%$ @ 100 °C		Does not include systematic uncertainties from specific application errors. Combine using RSS

* All values reported are assumed to be maximum values, i.e. those with over 99% coverage. It is therefore appropriate to multiply these values by two thirds to obtain values suitable for a 95% confidence.

** All random uncertainties repeated are maximum values, i.e. those appropriate for 99% coverage or about three standard deviations therefore all values should be divided by three to obtain one standard deviation

5.1.2 Calorimeter Temperatures

In addition to the overall TC DAQ system, the systematic error associated with the TC measurements on the inside (unheated) surface of the calorimeters has to be included. An intrinsic TC measurement normally involves attaching the TC junction directly to the measurement surface, ensuring a very fast (~0.1 s) time response. Intrinsic TC measurements are the most accurate method known for TC measurements, and are thought to be accurate to within a few K (this is supported by the recent work of Nakos et al. [2004]). Assuming a relatively large value of ±2 K, the error from this source is about 0.16% at 1273 K and 0.54% at 373 K, and is a systematic uncertainty. If this source is combined with other systematic uncertainties, the overall error at 1273 K does not change. The uncertainty at 373K increases slightly to about ±3.2 K or 0.9%.

The inside of the calorimeter is insulated and temperatures inside the outer shell of the calorimeter change slowly relative to the thermal response of the TCs. The very fast time response of intrinsic TCs is not required in this situation, so sheathed TCs, rather than intrinsic TCs are used to measure calorimeter temperatures in the radiation partitioning experiments. Nakos et al. [2004] showed that intrinsic TCs, are more accurate than MIMS TCs and that error in MIMS TCs increases roughly linearly with TC diameter. Based on recent work [Nakos et al., 2004; Nakos, 2004], a total uncertainty of ±2% for 40 mil TCs in the calorimeter will be assumed throughout the measurement range of these experiments. This uncertainty estimate is valid if the additional error due to mounting is less than 7 K at a temperature of 373 K and less than 25 K at a temperature of 1273 K.

5.1.2.1 Penlight Shroud Temperatures

The temperature of the Penlight shroud is measured by MIMS TCs mounted on the surface of the shroud. These TCs are exposed to convective air currents and radiation exchange with cool objects, such as the cylindrical calorimeter or the surroundings as seen through the annulus. However, the dominant radiation exchange is from the shroud to objects within the cavity and convection heat transfer from the TCs is not expected to be large, especially for test cases in which airflow into the annulus is restricted. Nakos et al. [2004] found that measurement errors for a 1/16 in. MIMS TC mounted on a flat shroud at 1300 K were approximately 120 K when the shroud was radiating to 300 K surroundings but less than 40K when radiating to a 700 K target. These radiation errors are likely to be less significant in the present series of tests because of the lower shroud temperatures (due to the nonlinear dependence of heat flux on temperature) and TCs in the cylindrical Penlight shroud will always see incident radiation from other parts of the shroud and the cylindrical calorimeter. Uncertainties for the 1/16 in. MIMS TCs on the Penlight shroud are therefore assumed to be the same as the calorimeter TC measurements, approximately ±2% over the entire measurement range.

5.1.3 Penlight Convective Flow Temperature Measurements

The temperature of the convective flow in Penlight is measured by an aspirated TC and/or two TCs of different sizes. The temperature of cool air in a strongly radiative environment will be overpredicted by aspirated as well as non-aspirated TCs. Uncertainties in aspirated TC measurements depend upon the temperature and suction velocity of the gas as well as the radiation intensity of the surroundings and the orientation of the radiation shield opening (see Blevins and Pitts [1999]).

Blevins and Pitts [1999] showed that the errors in TC readings are strongly dependent on the gas temperature, velocity, and the effective surrounding radiation temperature (T_∞). Table 5-2 gives the expected temperature difference (see Eq. (2.1)) between a TC and the air surrounding it, assuming an air temperature of 100ºC and velocity of 0.5 m/s. The data for bare bead and aspirated TCs are taken from plots presented by Blevins and Pitts; the MIMS TC data are solutions of the energy balance of Eq. (2.1) using the convection coefficient correlation of Eq. (2.2). The data presented are for order-of-magnitude estimates only. The conditions of the experiment may lead to larger or smaller errors than those predicted by this analysis.

Table 5-2. Estimated Error in TC Readings in Air at 100ºC with a Velocity of 0.5 m/s.

TC application	Error when T_∞ = 300ºC	Error when T_∞ = 600ºC
20 mil (0.5 mm) MIMS TC	39ºC	220ºC
1/16 in. (1.6 mm) MIMS TC	69ºC	330ºC
1.5 mm spherical bare bead TC	40ºC	220ºC
Aspirated TC (velocity 5 m/s)	1ºC	20ºC

The theoretical analysis of Brohez et al. [2004] suggests that the total variation in the radiation correction factor may be less than 20% for a quasi-steady flow and radiation environment over a broad range of operating conditions. However, the data presented by Brohez et al. [2004] indicates that the actual variation of the correction factor is very large, which may be partially due to

departures from a quasi-steady environment. When the quasi-steady assumption does hold, the key uncertainties in determining the correction factor are the uncertainty in convection coefficient and/or the effective surrounding temperature (see Eqs. (2.4) and (2.5)). Further analysis is required to determine the actual uncertainties in the Penlight application, but correlations for convection coefficients are typically subject to uncertainties on the order of 20%. Uncertainties in determining the flow velocity and temperature will compound this uncertainty. It appears likely that the uncertainty in the correction factor will be on the order of 50% in the Penlight application.

The error in aspirated TC measurements drops asymptotically as the aspiration velocity is increased; however, large aspiration velocities may change the flow field in Penlight so significantly that interpretation of the experimental results will become difficult. This is expected to be the case at high aspiration velocities, especially when the ends of the Penlight annulus are covered by insulation which would otherwise restrict the air flow into and out of the annulus.

5.2 CARS Convective Flow Temperature Measurements

Typical uncertainties in single-laser-pulse CARS temperature measurements in laboratory flames range from 3-5%, with some reduction in uncertainty when the CARS spectrum is averaged over many laser pulses. The chief source of uncertainty in CARS temperatures is mode-amplitude noise in the output of the broadband Stokes dye-laser source. If time permits, S NL will investigate the feasibility of a modeless laser oscillator for improved noise performance. A more detailed assessment of measurement uncertainty in the measurements at FRH will be conducted following acquisition of CARS data from the facility.

5.3 Convective Flow Velocity Measurements

5.3.1 Velocities in FRH

Uncertainties in a PIV system, such as the one used to measure velocities in the near field around the calorimeter in FRH, are typically 1 to 2% when used in a laboratory setting. At larger scales nd field implementations, the uncertainty is expected to increase to approximately 5 to 10%. Sources of uncertainty are primarily due to improper correlation during PIV analysis and averaging of velocity gradients within the interrogation region (measurement area). Both of these error sources can be reduced by seeding the flow with PIV seed particles in a uniform, steady manner. This will require some design and testing for the new FRH application.

5.3.2 Velocities in Penlight

The convective flow velocity in the axial direction in Penlight is measured with a differential pressure gauge coupled with a pressure transducer. For a known density and differential pressure, the velocity can be determined to within the uncertainty in the calibration constant for the differential pressure probe. The uncertainty in the calibration constant is less than approximately 8% when the probe Re is greater than 600, corresponding to a velocity of approximately 0.36 m/s at room temperature. At lower Re the constant becomes a function of Re, and uncertainty in the

calibration becomes large when the probe Re drops below 400 [Kent and Schneider, 1987]. The expected Re of the probe in the experiments in Penlight is less than 400 due to the low velocities of the natural convection flow field.

Uncertainty in the temperature of the air at the probe contributes to overall uncertainty through its influence on Re. For an ideal gas, the density is inversely proportional to the absolute temperature. Neglecting temperature effects on Re through the temperature dependence of viscosity, the percentage uncertainty in velocity is proportional to half the percentage uncertainty in absolute temperature. Combining this uncertainty with the uncertainty in the calibration constant, assuming Re greater than 600, a maximum uncertainty of ±30 K in the aspirated TC or corrected two-TC measurement and an air temperature of 373 K, the total uncertainty increases to 9%.

Uncertainties in the pressure transducer readings also contribute to the overall uncertainty. The range of the pressure transducer is ±0.05 in. WC (±12 Pa), and the uncertainty of the pressure transducer is 0.4% of full scale (0.4% FS), which corresponds to 0.0004 inches WC at 70ºF (0.1 Pa at 21ºC). The uncertainty increases as the difference in temperatures from this reference point increases, at a rate of 0.033% FS/ºF (0.059% FS/ºC) over the range 0ºF to 150ºF (32ºC to 66ºC). This source of uncertainty is likely to be small relative to the uncertainty in air density and probe calibration constant.

5.4 Heat Flux Measurements

5.4.1 Medtherm HFGs

5.4.1.1 Total HFG

An equation relating the output of a Schmidt-Boelter total HFG to the net absorbed heat flux due to convection and radiation is given in Eq. (5.1) [Nakos, 2005]. In this equation, q_{net} is the net heat flux into the gauge, mV is the output signal from the gauge, K refers to a calibration constant and F refers to a fraction of the total heat flux. The subscripts *rad* and *conv* refer to the radiative and convective components, respectively.

$$q_{net} = mV * \left(K_{rad} * F_{rad} + K_{conv} * F_{conv}\right) \tag{5.1}$$

Total HFGs such as the gauges used in the present report are typically calibrated in an environment in which the radiative heat flux dominates. However, there is evidence [Diller, 2004] that the calibration constants of the radiative and convective components may differ, and that the convective calibration constant may not in fact be a constant but may depend upon details of the convective flow. The manufacturer's calibrations for the four dual (total and radiative) HFGs in the cylindrical calorimeter are included in Appendix B. Uncertainty of the gauge, per the manufacturer, is ±3% of the responsivity, corresponding to a measurement uncertainty for the total HFG of ±3% of the measurement across the calibration range of 0 to 150 kW/m^2. This uncertainty, however, is based on a calibration methodology which uses only a radiative heat source. In the present work, we will assume that the manufacturer's calibration has determined the calibration constant of the radiative, rather than the total, heat flux to within the manufacturer's estimated uncertainty.

Diller [2004] measured the convective calibration constant of a similar Medtherm dual heat flux gauge and found the calibration constant in a convection-dominated environment to be approximately 12% lower than the manufacturer's calibration, with an uncertainty in the calibration constant of ±20%. In the absence of a known calibration constant for the convective heat flux of the gauges used in the present experiments, the calibration constant of the convective fraction will be assumed to have the same relationship to the radiative calibration constant as the gauge calibrated by Diller. The overall uncertainty for Schmidt-Boelter total heat flux gauges has been estimated to be ±23% for the net absorbed heat flux and ±39% for the incident heat flux under conditions similar to those of the present experiments [Nakos, 2005].

Additional sources of uncertainty include calibration uncertainty in the DAS, voltage drop across the wires connecting the Medtherm gauge to the DAS, etc. The calibration was checked by inputting a known voltage through an Ectron into the DAS plug board, similar to the TC calibration using the Ectron as discussed in Section 5.1.1. The wires are 25 ft (7.6 m) in length, 24 gauge thickness, and are twisted in pairs and shielded. Passive sensors such as thermopile gauges measure a differential voltage with very low current and are not sensitive to voltage drop in the wiring. The uncertainty due to the DAS and wiring are therefore expected to be small. The total uncertainty in determining the total incident heat flux will be assumed to be ±40% in both Penlight and FRH.

5.4.1.2 Radiometer

The radiative HFGs are radiometers, designed to be sensitive only to the absorbed radiative heat flux. The relationship of the net heat flux to the gauge output can be expressed as in Eq. (5.1) with K_{conv} and F_{conv} set to zero. The calibration constant of the radiative heat flux can then be determined through a calibration procedure carried out in a radiation-dominated environment. The uncertainty of the calibration is not subject to the ambiguity of multiple calibration constants discussed in the preceding section, and the manufacturer's uncertainty estimates will be applied in the present work.

The manufacturer's calibration curves for the radiometers are similar to the total HFG curves (see Appendix B). Uncertainty, per the manufacturer, is again ±3% of the responsivity, corresponding to a measurement uncertainty for the radiative HFG of ±3% of the measurement across the calibration range of 0 to 150 kW/m^2. Additional sources of uncertainty for the radiometer due to voltage drop in the wires, calibration of the DAS, etc., are the same as for the total HFG. Although these sources of uncertainty are not large, the total uncertainty in the net radiative flux will be assumed to be ±5% in the present work.

The uncertainty in the incident radiative flux is larger than the uncertainty in the net absorbed flux due to the uncertain gauge temperature and emissivity. An analysis similar to that performed by Nakos [2005] for Schmidt-Boelter total heat flux gauges can be performed on a Schmidt-Boelter radiometer with the assumption that there is no convective heat transfer to the radiometer. If the gauge emissivity is taken to be that of Pyromark 2500, the gauge temperature is taken to be the temperature of the cooling water with an uncertainty of ±10%, and the uncertainty in the net radiative flux is ±5%, the total uncertainty in the incident radiative flux is ±10%

when the net flux is 5 kW/m^2 and ±11% when the net flux is 30 kW/m^2. For the present work, the total uncertainty of the incident radiative flux measurements for the radiometer will be assumed to be ±15% to add some conservatism.

5.4.2 Heat Flux Measurements made by Beck Engineering IHCP1D

The heat flux incident on the calorimeter surface can also be calculated using a 1-D inverse heat conduction methodology. In the method, one or more TC measurements is used to estimate absorbed heat flux using known boundary conditions, material properties and dimensions. The total absorbed flux is captured via this method: both radiative and convective. One can add a term approximating the energy reradiated to obtain a measure of the heat flux incident flux. Parameter values used to estimate the incident heat flux are uncertain.

Figueroa et al. [2005] estimated the maximum uncertainty in heat flux using the inverse heat conduction program IHCP1D (Beck Engineering & Associates) to be about ±20% for a cylindrical calorimeter near, but not in, a fire. Nakos [2005] showed that the incident flux uncertainty could be as large as ±40% in situations broadly similar to those of the present experiments. An uncertainty of ±40% will be assumed for the present experiments both in Penlight and in FRH.

5.4.3 Convective Heat Flux Measurements

The convective heat flux will be estimated from the convective flow velocities and temperatures (Eq. (5.2)). A convective heat transfer coefficient (h) is measured or estimated from the temperature and velocity of the gas free-stream by means of an appropriate empirical correlation. Uncertainties in correlations are typically on the order of 25%; an uncertainty of 35% will be assumed in the present work because classical correlations may not directly apply to the experimental conditions of the present experiments. If uncertainties in free-stream and surface temperatures are assumed to be 10%, the overall uncertainty of the convective heat transfer is approximately 40% at the highest expected heat transfer rates (Table 5-3). In this table, a convective heat transfer coefficient (h) of 15 kW/m^{2}K was assumed. Note that the percentage of uncertainty is greater when the difference between the surface and gas temperatures is small.

$$q_{conv} = h*\left(T_{gas} - T_{surf}\right) \tag{5.2}$$

Table 5-3. Uncertainties in Convective Heat Flux.

T_{gas} (K)	T_{surf} (K)	q_{conv} (kW / m^2)	Uncertainty (kW / m^2)	% Uncertainty
473	353	1.50	1.05	70
873	353	7.50	2.99	40
1473	353	16.50	6.21	38

5.5 Fuel Regression Measurements

An uncertainty analysis was performed using the method described by Coleman and Steele [1999]. The uncertainty for fuel regression concentrates on the systematic uncertainty. Parameters contributing to the systematic uncertainty are primarily based on manufacturer's specifications. Contributions to the error include the pressure measurement uncertainty (0.4% for

temperature changes no greater than 50ºF (28ºC)), the time measurement uncertainty (0.03%), and the fuel specific gravity measurement uncertainty (0.5%), all taken as a percentage of the upper limit of the gauge. The calculated total uncertainty in the fuel regression measurement due to systematic uncertainty is 0.15 in. WC, 0.6% of the maximum value for the gauge.

5.6 Measurement Uncertainty Summary

Table 5-4 summarizes the measurement uncertainties for these types of experiments. Due to the ny approximations made, the calculated uncertainties are rounded up to add some conservatism. A post-test uncertainty analysis will be performed after the experiments to test the assumptions of the pre-test analysis and further quantify the uncertainty of the measurements.

Table 5-4. Measurement Uncertainty Summary.

Measurement Type	Maximum Total Uncertainty	Comments
1) TC measurements	±2.6K at 373K or ±5.5K at 1273K	Does not include systematic errors due to mounting, etc.
2) Penlight shroud temperatures	Approximate by ±2% at all temperatures	Systematic errors due to mounting are largest contributor
3) Calorimeter temperatures	Approximate by ±2% at all temperatures	Systematic errors due to mounting are largest contributor
4) Total heat flux from Beck Engineering IHCP1D code	Approximate by ±40% at all heat flux levels	Uncertainties may be higher during periods of rapid temperature change
5) Medtherm HFG total heat flux estimates	Approximate by ±40% of measurement in Penlight or FRH	Uncertainty increases as convection becomes more important
6) Medtherm HFG radiative heat flux estimates	Approximate by ±15% of measurement	
7) Convective heat flux estimates	±40% of the convective component at the highest expected flux levels	Uncertainties (expressed as a percentage of the convective heat flux) are highest when the convective heat flux is small
8) Aspirated TC air measurements	On the order of 20K at aspiration velocities of 5 m/s	Aspiration may significantly alter the flow field
9) 2-TC air temperatures	Uncorrected measurements subject to bias errors on the order of 300K Correction factor uncertainty estimated 50% at steady state	Further analysis required for uncertainty of radiation correction of MIMS TCs in Penlight
10) Velocities from differential pressure	±8% at room temperature for probe Re > 600. ±9% at 373K for an assumed temperature uncertainty of 30K	Uncertainties in Penlight experiments will likely be much larger due to probe calibration uncertainty in the low Re range
11) Velocities from PIV	1-2% when applied under ideal laboratory circumstances. Up to 10% for FRH implementation	Based on experience with PIV in both laboratory and old FLAME settings. Uncertainty will be reduced by careful seed particle introduction (the more uniform the better)

Table 5-4. Measurement Uncertainty Summary.

Measurement Type	Maximum Total Uncertainty	Comments
12) Temperatures from CARS	3-5% of the measured absolute temperature for single-pulse realizations. 2-3% for averaged temperatures	Estimate is based on experience and previous reports. Noise performance is system-dependent and will be reassessed when data from FRH are available
13) Fuel Regression	±1% of maximum value	0-25 inches WC

6. REFERENCES

Blanchat, T., Luketa-Hanlin, A., Romero, C., Tieszen, S., and Romero, V., "Plan to develop validation data for heat flux to a complex object in a fire plume for the SYRINX/FUEGO/CALORE fire and thermal response codes," SAND2005-3912, August 2005, Sandia National Laboratories, Albuquerque, NM.

Blevins, L. G., and Pitts, "Modeling of bare and aspirated thermocouples in compartment fires," *Fire Safety Journal*, Vol. 33, 239-259, 1999.

Brohez, S., Delvosalle, C., and Marlair, G., "A two-thermocouples probe for radiation corrections of measured temperatures in compartment fires," *Fire Safety Journal*, Vol. 39, 399-411, 2004.

Brown, A. L., "Pretest Simulation of a Cylindrical Calorimeter in a 2-m Methanol Fire using FUEGO," Sandia internal memo to T. Blanchat and distribution, May 24, 2006.

Bryant, R., Womeldorf, C., Johnsson, E., and Ohlemiller, T., "Radiative heat flux measurement uncertainty," *Fire and Materials*, Vol. 27:209-222, 2003.

Coleman and Steele. *Experimentation and Uncertainty Analysis for Engineers*, Wiley & Sons, 1999.

Diller, T., Virginia Tech University, Informal communication to Blanchat, T. K., Sandia National Laboratories, May 2004.

Figueroa, V. A., Nakos, J. T., and Murphy, J. E., "Uncertainty analysis of heat flux measurements estimated using a one-dimensional inverse heat conduction program," SAND2005-0339, February 2005, Sandia National Laboratories, Albuquerque, NM.

Incropera, F. P., and DeWitt, D. P. *Fundamentals of Heat and Mass Transfer*, 4th edition, Wiley & Sons, 1996.

Kearney, S. P., and Jackson, M. N., "Dual-pump CARS thermometry in sooting acetylene-fueled flames," 44th AIAA Aerospace Sciences Meeting and Exhibit, 9-12 Jan., 2006, Reno, NV.

Kent, L. A., and Schneider, M. E. "The design and application of bi-directional velocity probes for measurements in large pool fires," *ISA Transactions*, Vol. 26, No. 4, 25-32, 1987.

Lopez, C., Koski, J. A., and Razani, A., "Estimate of error introduced when one-dimensional inverse heat transfer techniques are applied to multi-dimensional problems," in *Proceedings of Numerical Heat Transfer Conference*, NHTC2000-12037, Pittsburgh, Pennsylvania, August 2000.

Nakos, J. T., "Uncertainty analysis of thermocouple measurements used in normal and abnormal thermal environment experiments at Sandia's Radiant Heat facility and Lurance Canyon burn site," SAND2004-1023, April 2004, Sandia National Laboratories, Albuquerque, NM.

Nakos, J. T., Suo-Anttila, and Gill, W., "Shroud boundary condition characterization experiments at the Radiant Heat Facility," SAND2004-5080, October 2004, Sandia National Laboratories, Albuquerque, NM.

Nakos, J. T., "Uncertainty analysis of steady state incident heat flux measurements in hydrocarbon fuel fires," SAND2005-7144, December 2005, Sandia National Laboratories, Albuquerque, NM.

O'Hern, T. J., Weckman, E. J., Gerhart, A. L., Tieszen, S. R., and Schefer, R. W., "Experimental study of a turbulent buoyant helium plume," Journal of Fluid Mechanics, 544, 143-171, 2005.

Pitts, W. M., Braun, E., Peacock, R. D., Mitler, H. E., Johnsson, E., Reneke, P. A., and Blevins, L. G. "Temperature uncertainties for bare bead and aspirated thermocouple measurements in fire environments," *Proceedings of the Joint Meeting of the Combustion Institute*, 508-511, March 1999.

Ricks, A. J., "Characterization of air flow in New FLAME / Radiant Heat," Sandia internal memo to T. Blanchat, March 20, 2006.

Robertson, A. F., and Ohlemiller, T. J., "Low heat-flux measurements: some precautions," *Fire Safety Journal*, Vol. 25, 109-124, 1995.

Romero, V. J., Sherman, M. P., Dempsey, J. F., Edwards, L. R., Chen, K. C., Baron, R. V., King, C. F., "Development and illustration of model validation concepts on a component failure model," paper AIAA-2004-1991, *45th AIAA/ASME/ASCE/AHS/ASC Structures, Structural Dynamics, and Materials Conference*, April 19-22, 2004, Palm Springs, CA.

Romero, V. J., Sherman, M. P., Johnson, J. D., Dempsey, J. F., Edwards, L. R., Chen, K. C., Baron, R. V., and King, C. F., "Development and validation of a component failure model," paper AIAA2005-2141, *46th AIAA/ASME/AHS/ASC Structures, Structural Dynamics, and Materials Conference*, April 18-21, 2005, Austin, TX.

Tieszen, S. R., O'Hern, T. J., Schefer, R. W, Weckman, E. J., and Blanchat, T. K., "Experimental study of the flow field in and around a one meter diameter methane fire," *Combustion and Flame*, 129(4), 378-391, 2002.

Tieszen, S. R., O'Hern, T. J., Weckman, E. J., and Schefer, R. W., "Experimental study of the effect of fuel mass flux on a one meter diameter methane fire and comparison with a hydrogen fire," *Combustion and Flame*, 139(1-2), 126-141, 2004.

Tieszen, S. R., personal communication, May 2006.

Trucano, T. G., Pilch, M., and Oberkampf, W. L., "General concepts for experimental validation of ASCI code applications," SAND2002-0341, March 2002, Sandia National Laboratories, Albuquerque, NM.

Wetterlund, I., and Persson, B., *Calibration and use of heat flux meters*, Vol. 1, pg. 35, Interscience Communications Ltd., London, England, 1999.

Zhukauskas, A., "Heat transfer from tubes in cross flow," in J. P. Hartnett and T. F. Irvine, Jr., Eds., *Advances in Heat Transfer*, Vol. 8, Academic Press, New York, 1972.

APPENDIX A:
PRETEST SIMULATION OF A CYLINDRICAL CALORIMETER IN A 2-M METHANOL FIRE USING FUEGO

Sandia National Laboratories
Operated for the U.S. Department of Energy by
Sandia Corporation

Albuquerque, New Mexico 87185-1135

date: **24 May, 2006**

to: **Distribution**

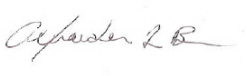

from: **A. L. Brown***

subject: **Pretest Simulation of a Cylindrical Calorimeter in a 2-m Methanol Fire using FUEGO**

Introduction

A series of tests have been commissioned to test a cylindrical calorimeter in the new flame facility. The fire in question is a methanol fuel fire. The fuel pan is 2 meters in diameter. Since these are to be validation tests, a pre-test prediction is necessary to conform to minimum validation practice standards.

Fuego has been used to perform several calculations with the Flame facility geometry [1-3]. The geometry has been extracted from an existing CAD geometry file for the facility. The TFNS model is used for modeling the turbulence. A liquid pool evaporation model is used to predict the burning rate of the fuel. The EDC combustion and soot models are employed. A conjugate region is used to extract the response of the calorimeter. The calorimeter is modeled as a steel cylinder. A discrete ordinates model is employed for solving the participating media radiation.

This memo documents the pre-test predictions, and provides quantitative and qualitative estimates to help guide the design of the test.

Model

The geometry for this case was derived from a CAD drawing of the facility. Some clean-up and simplifications were necessary to make meshing the geometry tractable. Even in the CAD geometry, many geometric details of the facility were ignored. The basement was assumed clear of any obstacles. In reality, there are numerous facility related geometric details, like piping and instrument boxes. Also, the grating and floor support is ignored. The inlet to the facility was only modeled from the level of the basement floor in the facility. The outlet was only modeled to the point of convergence of the conical ceiling.

* Sandia National Laboratories, Fire Science and Technology, Dept. 1532

The meshes for this case were generated using version 10.0 of the Cubit software. Generating a mesh is typically an iterative process. Iteration is required to converge on a mesh that is sufficiently coarse for practical calculations, yet sufficiently fine in regions of interest. Although many meshes were created and tested for this problem, only two principal meshes are described herein. One will be termed a coarse mesh, and employs approximately 450,000 elements, and nominally 13-25 cm (5-10 inch) sized spacing around and below the calorimeter. The other is termed the fine mesh, and employs approximately 1.3 million elements, and nominally 10-13 cm (4-5 inch) sized spacing around and below the calorimeter. An illustration of the coarse mesh is found in Figure 1, and the fine mesh is found in Figure 2. A cylindrical block was employed for calculating solid object response. This was meshed with approximately 100,000 elements, and thermal properties for steel were employed for the object in the calculation from Holman [4].

The mesh files were exported in genesis format, and used in Fuego calculations. The mesh file was designed with sidesets that corresponded to a previous calculation performed for the Flame facility. The corresponding input deck was employed for this calculation with slight modifications. Boundary conditions include an 'open' boundary condition at the top of the facility, a velocity inlet condition at the bottom ring, and a mass injection boundary condition at the fuel pool. The velocity boundary condition was set with the inflow at 0.9 m/s, and low turbulence parameters. The ring is 61 cm (2 feet) wide, and around 17.4 meters (57 feet) in diameter. The assumed velocity results in an equivalent volumetric flow of approximately 67,000 CFM of air in the facility. Table 1 lists the parameters assumed for the fuel pool in the mass injection boundary condition. Properties were extracted for methanol near room temperature from Gerhart et al. [5]. The walls of the facility were modeled as wall boundary conditions in Fuego.

Table A-1. A Listing of the Mass Injection Boundary Condition Parameters.

Parameter	Value	Units
Initial pool height	8.0	cm
Initial pool temperature	298	K
Pool evaporation temperature	338	K
Pool absorption coefficient	1.0	
Pool heat of evaporation	1101	kJ/kg
Pool specific heat	2.37	kJ/kgK
Pool density	800	kg/m^3

Results and Discussion

Results from two cases are presented. The fine calculation was run on 128 Processors on the rogue computing cluster. The coarse calculation was run on 84 processors on the rogue computing cluster. Approximately 48 hours were employed for each calculation.

Figure 3 shows the predicted fuel regression rate for the fine calculation. Drysdale [6] suggests that the critical (maximum) fuel regression rate for a methanol fire is 1.7 mm/min based on a theoretical argument based on an empirical model. The results in the figure suggest a fuel regression rate that is just above the theoretical peak, or about 1.8 mm/min. The Fuego pool regression rate model and the best available literature estimate for the regression rate are in reasonable agreement. It is thought that for a pretest prediction that the pool regression rate model yields an acceptable first estimate of the fuel regression rate.

Simulations were run for at least 25 seconds. High resolution output was retained for the first 25 seconds. The fire took approximately 8 seconds to reach a pseudo-steady-state. Average values were therefore examined from 8-25 seconds of time at the 0.1 second time interval. Figure 4 shows coarse mesh predictions for the average temperature. Figure 5 shows average temperature predictions for the fine mesh on a centerplane and for 3-Dimensional iso-contours. Differences between the coarse and fine mesh predictions are subtle. Some moderate differences exist, in particular just above the calorimeter. The calorimeter does not appear to be fully engulfed, and surrounding temperatures are higher towards the center of the calorimeter than at the extremities. Also plotted in Figure 4 and 5 are iso-contours of temperature at 900 K. The flame height appears reasonable as estimated from the height of the 900 K contour. It is approximately 3 meters in height, or about 1.5 pool diameters.

The calorimeter environment is also examined. Figure 6 shows the average radiative heat flux predictions to the calorimeter averaged from 7.5 to 25 seconds at intervals of 2.5 seconds. The peak heat flux is found on the bottom of the calorimeter. Peak predicted flux is a little above 100,000 W/m^2. Curiously, the peak flux is not at the center, rather at an offset. Comparing this with the temperature contours (Figure 5), there is a corresponding peak in the predicted average temperature field at the same location. The predicted peak flux to the top of the cylinder is between 50,000 and 75,000 W/m^2.

Follow-up Calculation

The initial calculations did not include in the output variables the necessary information to analyze the convective or the total heat flux. The fine case was therefore re-visited with Version 2.3beta of Fuego. This case was run to 42.5 seconds with output every 2.5 seconds. The average values were obtained by averaging surface variables from 7.5 seconds until 42.5 seconds. The calculation included reporting of the variables necessary to provide boundary estimates to the experimental team. Figures 7-12 show final object temperature, average T_∞, Convective heat transfer coefficient, convective flux, incident radiative flux, and total incident flux respectively. Please note that the scale for Figure 10 is different from that of Figure 11 and 12. The convective contribution to the total flux is significantly lower than that of the radiation.

Figure 13 and 14 show average predicted velocity at the centerplane. The vectors in Figure 14 are not scaled to illustrate the predicted average direction at the low velocity magnitudes. The average values were taken from simulation results from 5.05 seconds to 14.35 seconds. Peak velocities around the cylinder are around 8 m/s. The scale was

taken with the peak facility velocity as the maximum, and the 14 m/s peak velocity is found high above the cylinder (above the plots in Figure 13 and 14). Figure 15 shows the temperature averaged across the same interval. Even though the simulation has strong transient features, the average values exhibit good symmetry

Conclusions

A set of scoping calculations has been performed with the Fuego code for the cylindrical calorimeter experiments. The prediction results appear to give reasonable estimates of the pool regression rate and flame height. Predicted radiative heat flux and gas temperatures are examined to provide the experimental team with an initial estimate of the environment. Results from two distinct meshes appear to yield similar predictions, suggesting the degree to which the results are mesh independent.

References

1. Fuego Users Manual, Sandia National Laboratories, 2006.
2. Fuego Theory Manual, Sandia National Laboratories, 2006.
3. Fuego Verification Manual, Sandia National Laboratories, 2006.
4. Holman, J.P. *Heat Transfer*, Seventh Edition, McGraw Hill, 1990.
5. Gerhart, P.M.; Gross, R.J.; and Hochstein, J.I., *Fundamentals of Fluid Mechanics*, Second Edition, Addison-Wesley Publishing Co., 1992.
6. Drysdale, D., *An Introduction to Fire Dynamics*, Second Edition, John Wiley and Sons, West Sussex, England, 1998.

Figures

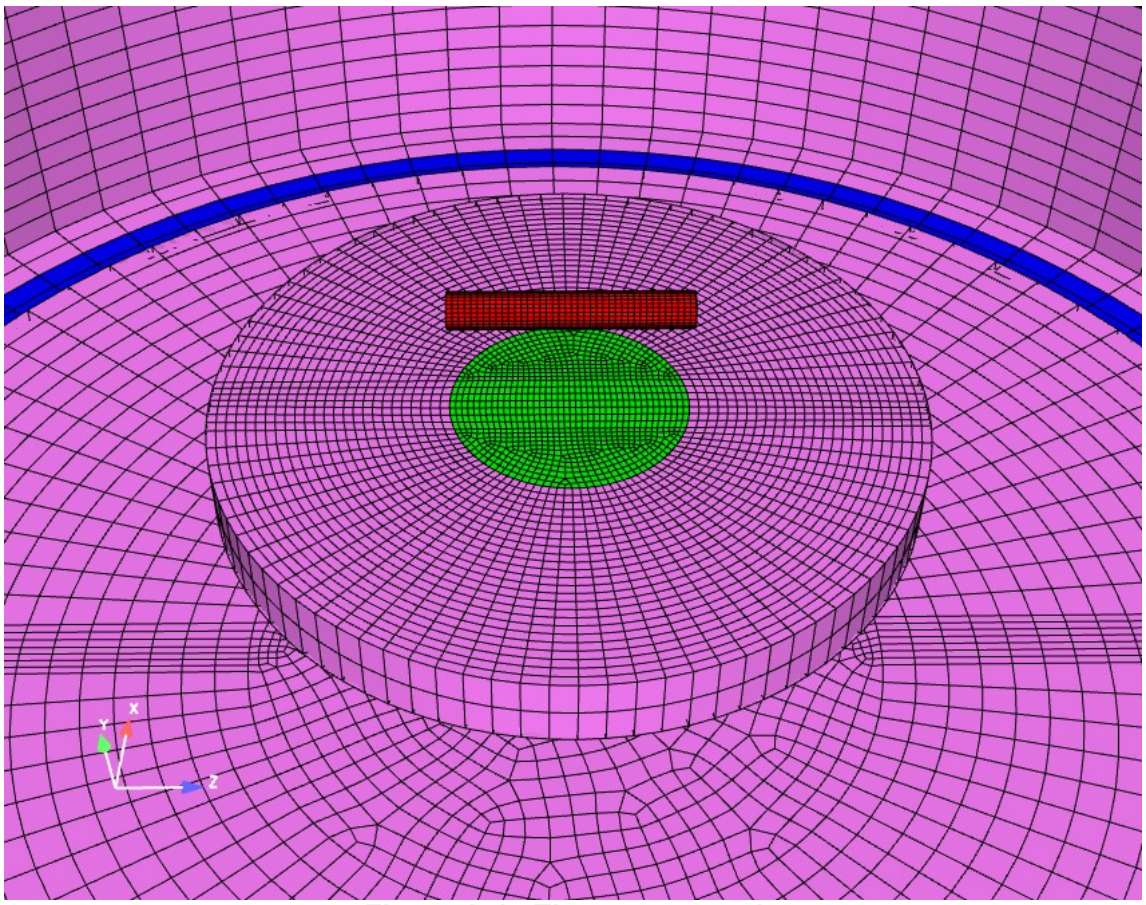

Figure A-1. The coarse mesh.

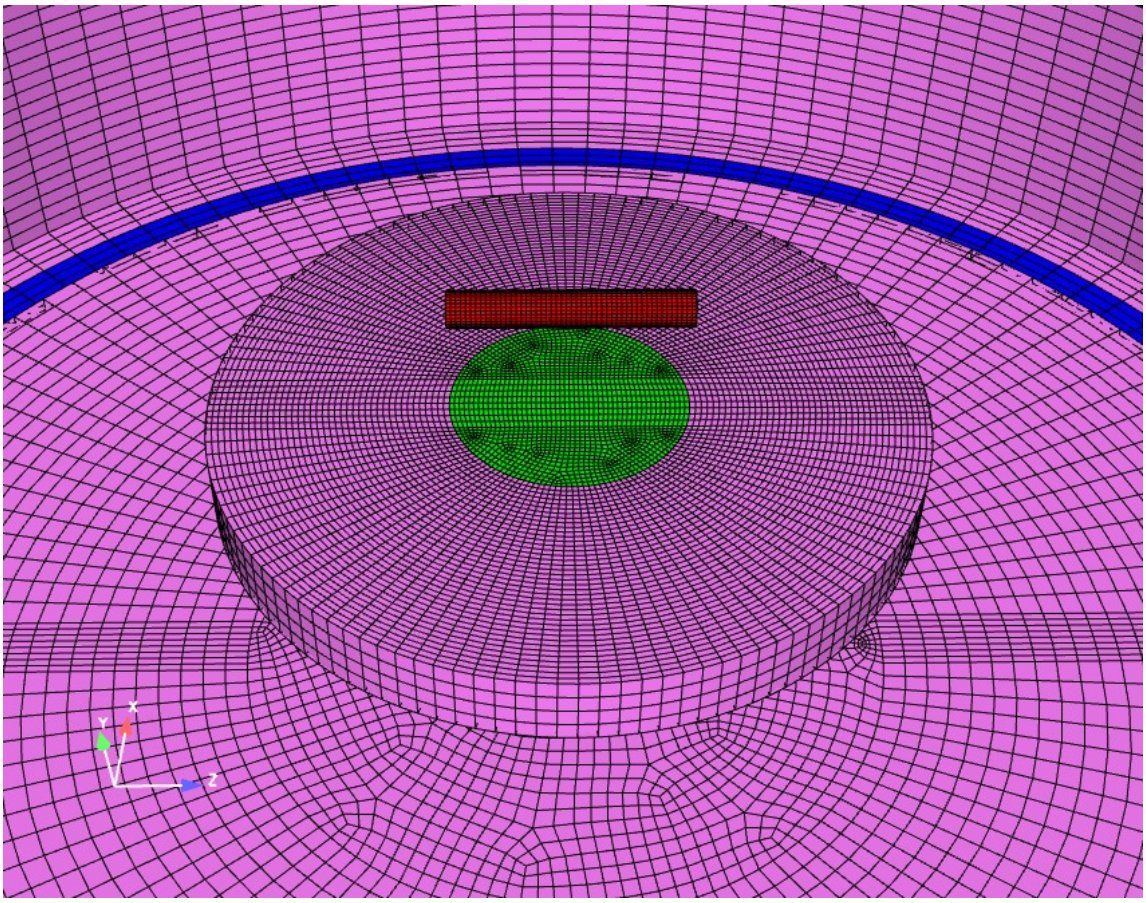

Figure A-2. The fine mesh

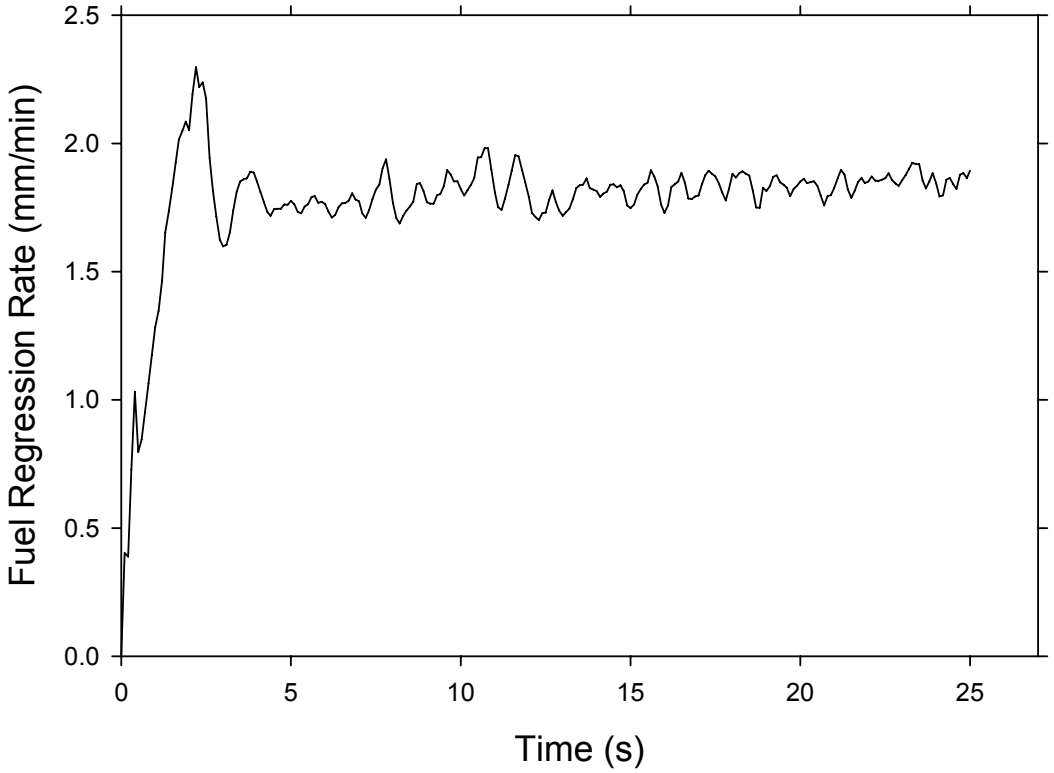

Figure A-3. The calculated fuel regression rate for the fine mesh.

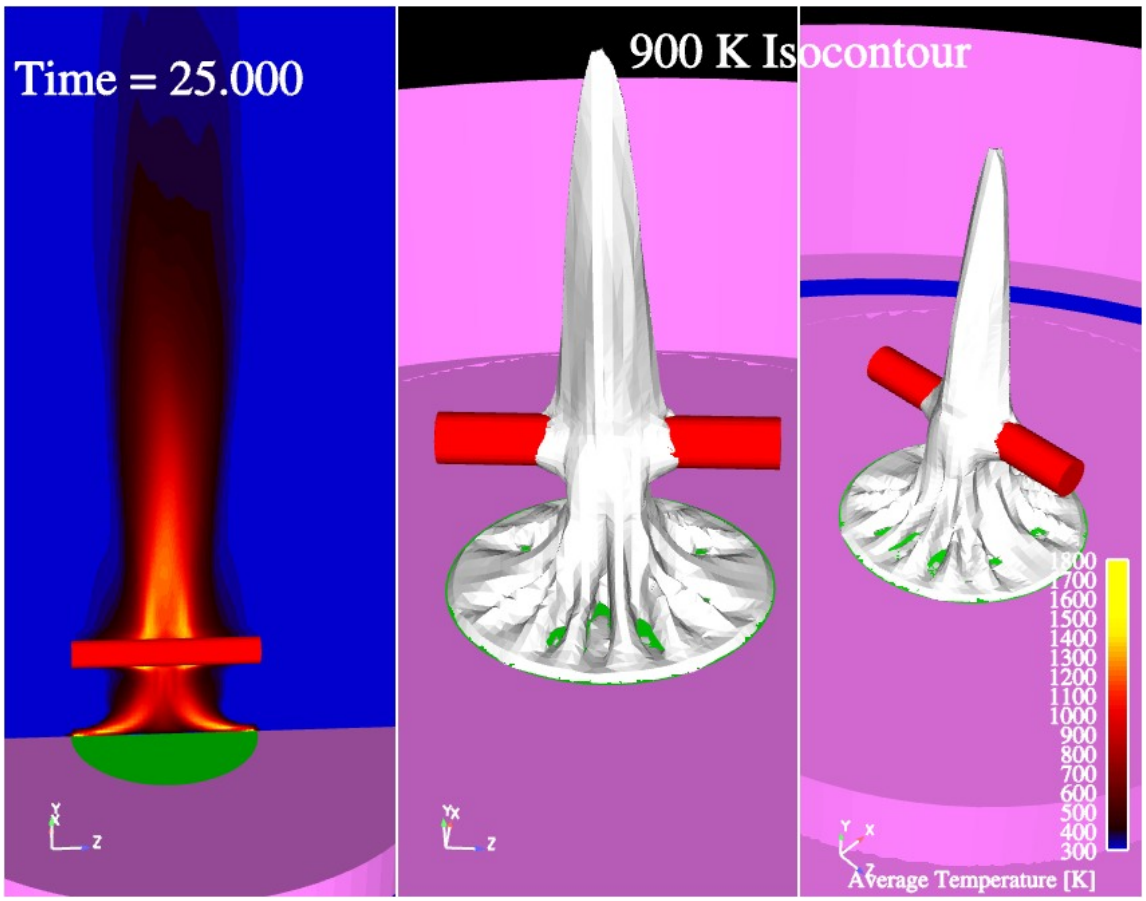

Figure A-4. Average temperature contours for the coarse mesh.

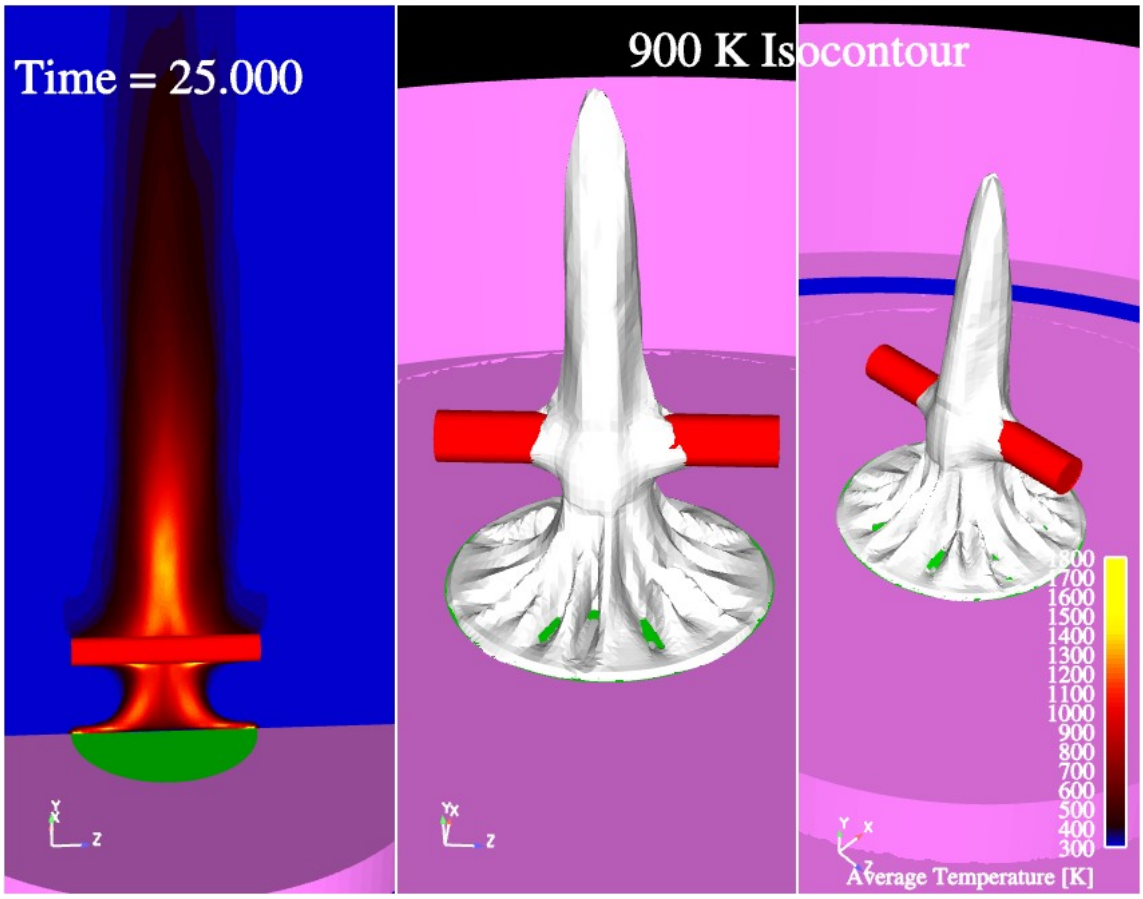

Figure 5. Average temperature contours for the fine mesh.

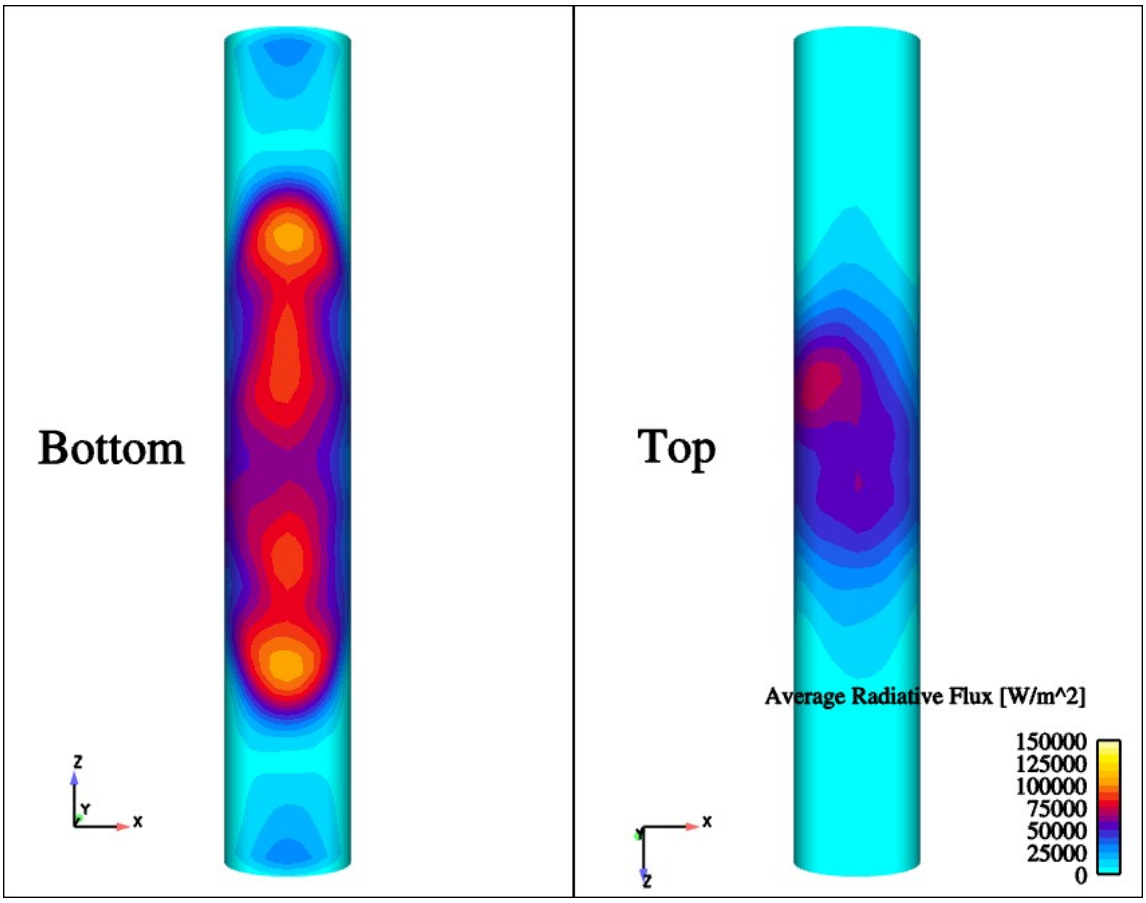

Figure A-6. Average radiative flux to the calorimeter for the fine mesh case.

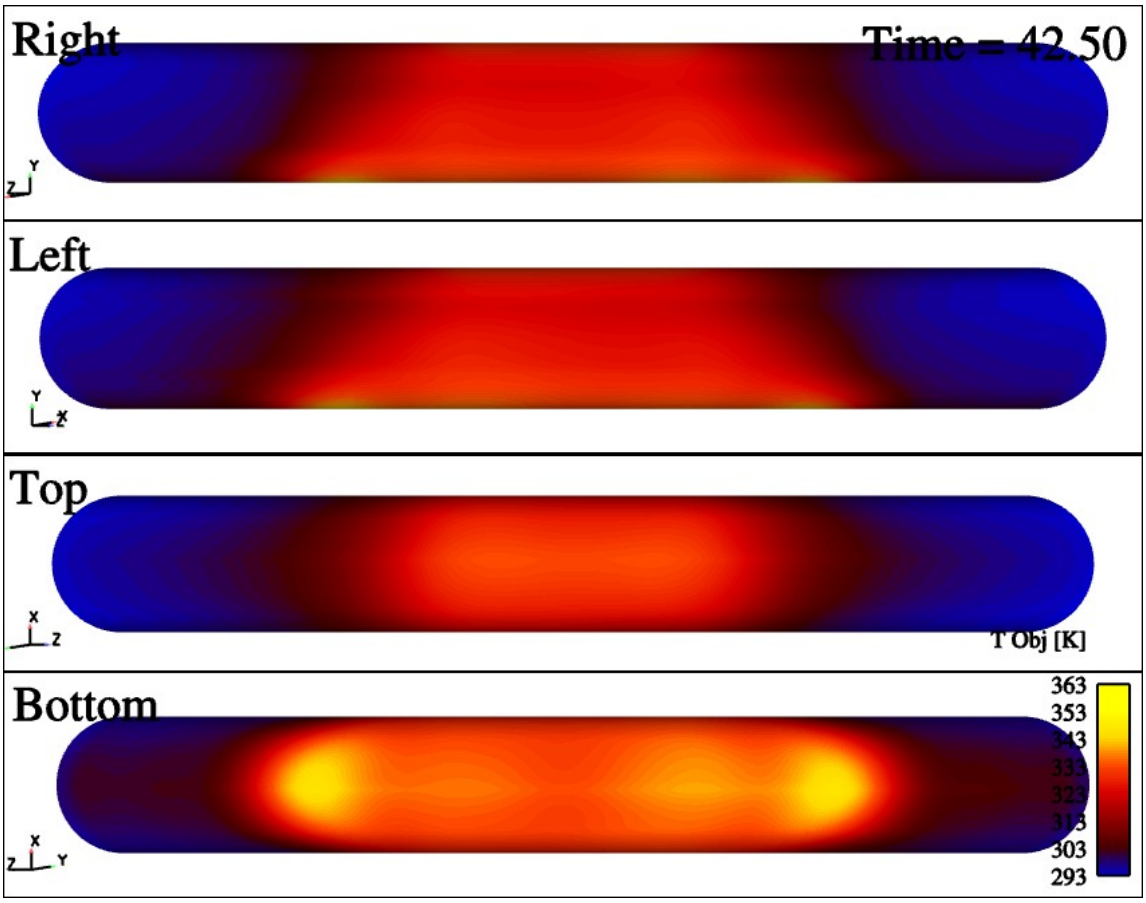

Figure A-7. Final predicted surface temperature on the calorimeter for the fine mesh case

.

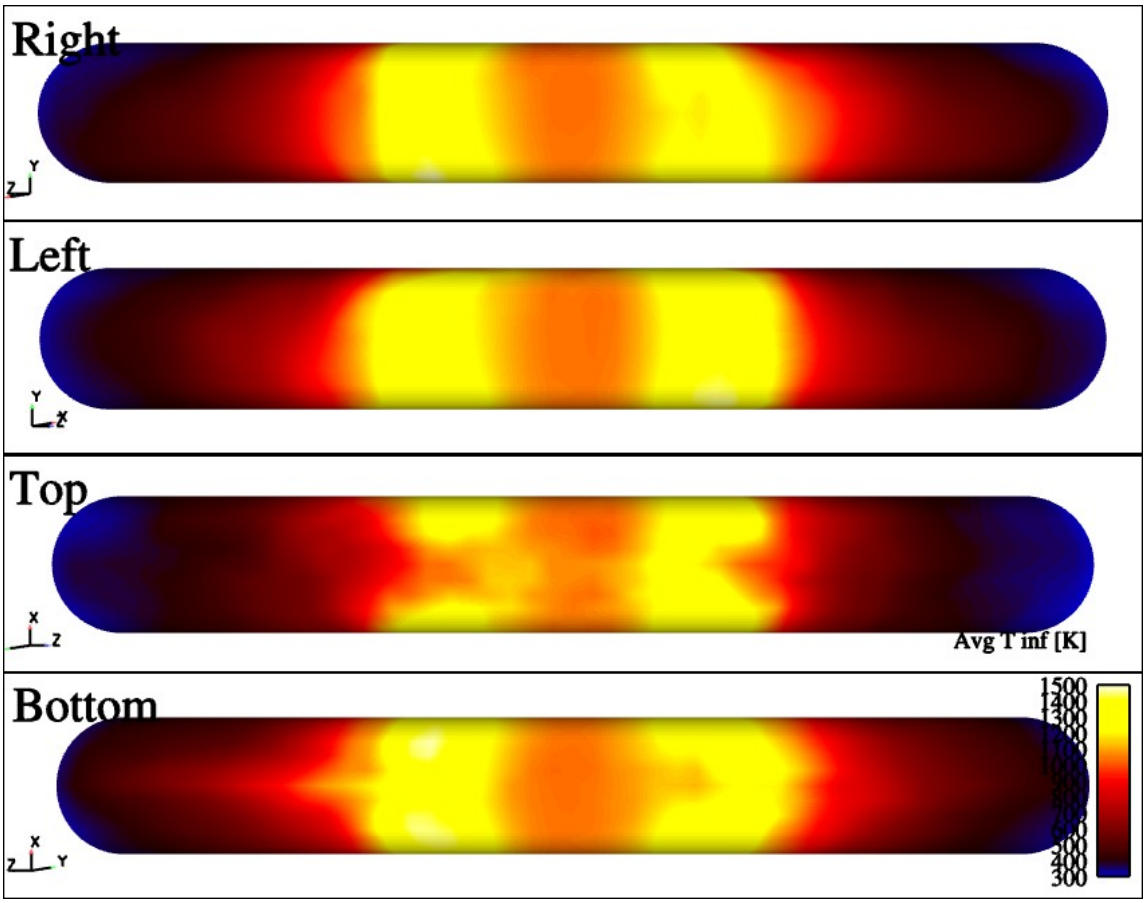

Figure 8. Average free-stream temperature around the calorimeter for the fine mesh case

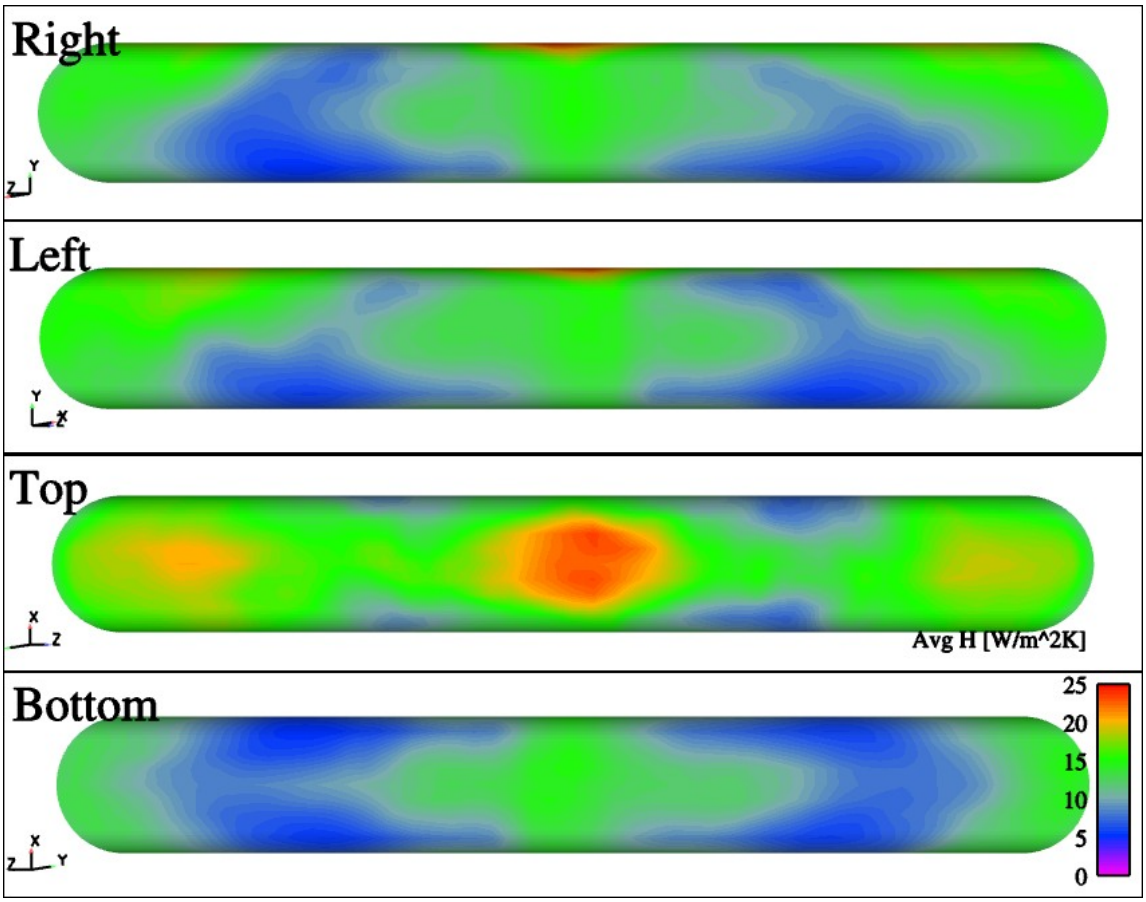

Figure 9. Average convective heat transfer coefficient at the calorimeter surface for the fine mesh case

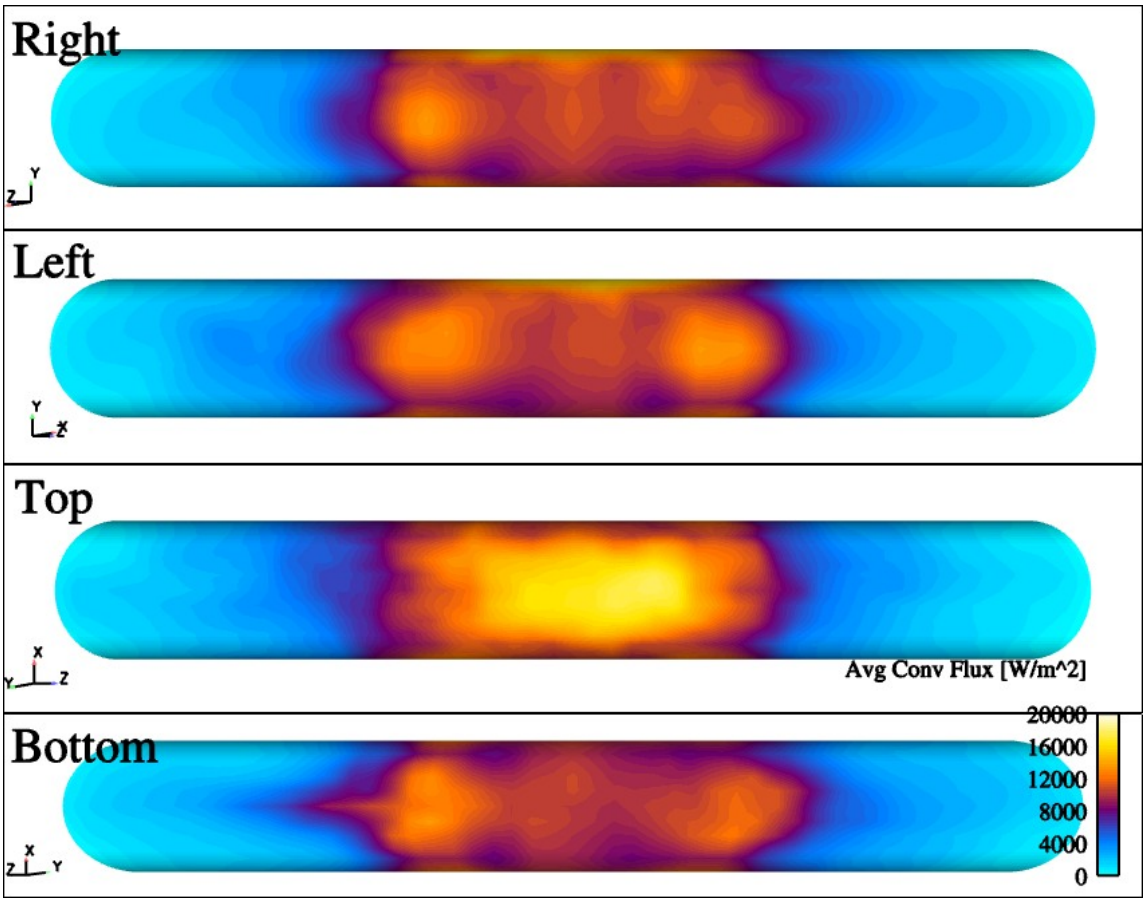

Figure A-10. Average convective heat flux at the calorimeter surface for the fine mesh case

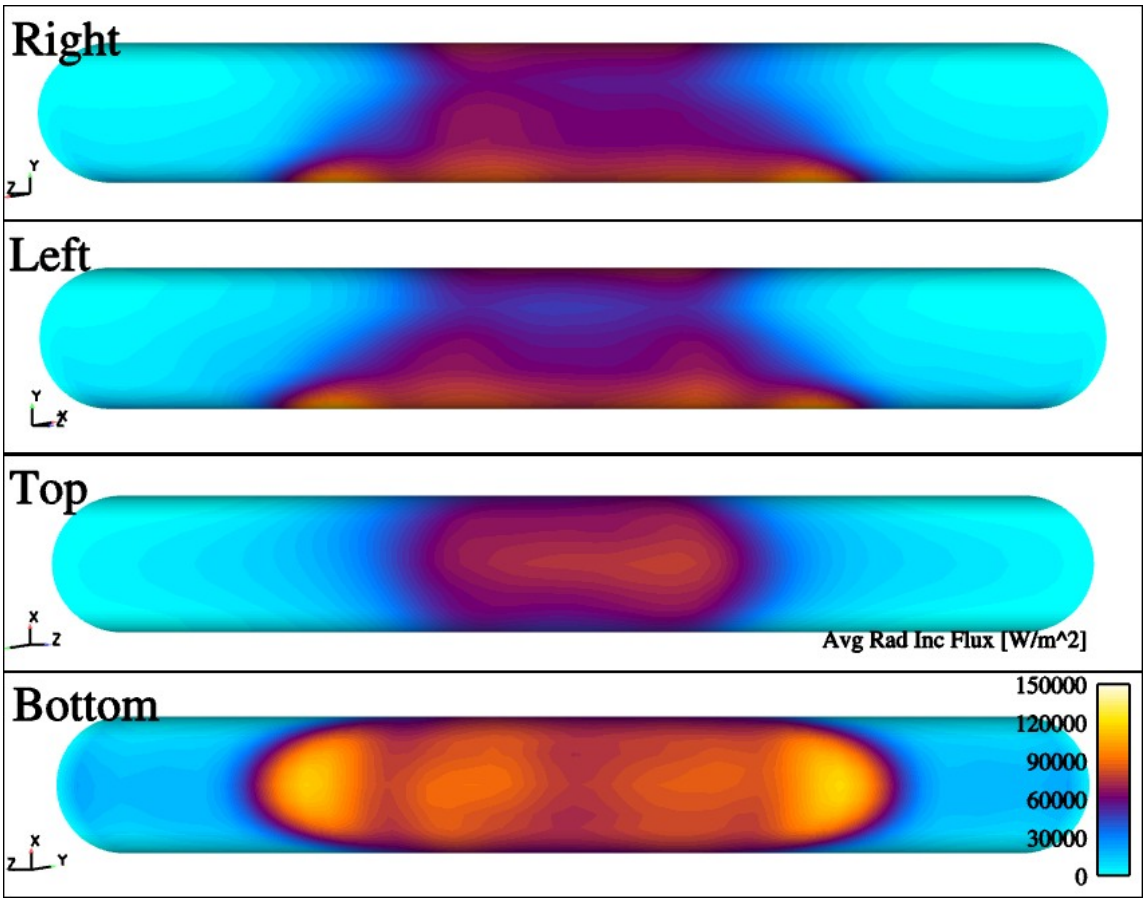

Figure A-11. Average incident radiative heat flux at the calorimeter surface for the fine mesh case

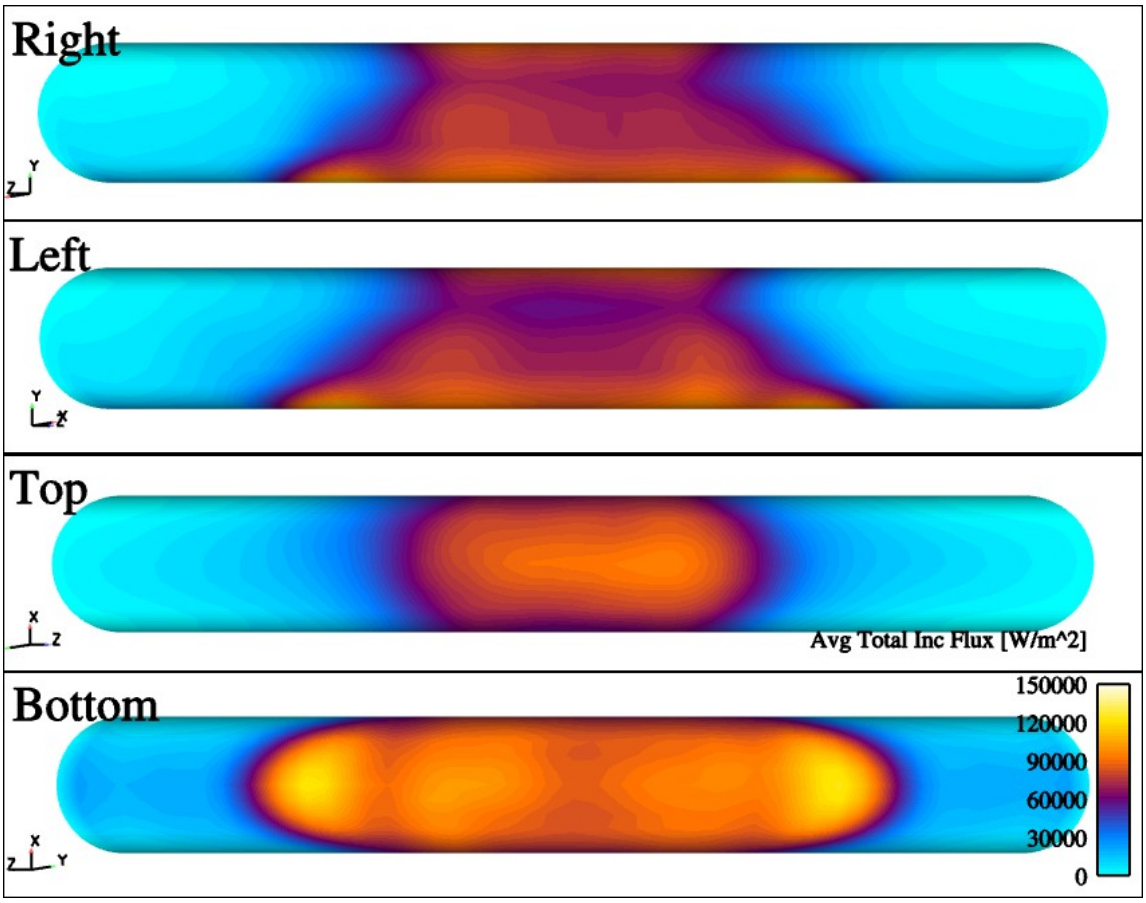

Figure A-12. Total incident heat flux at the calorimeter surface for the fine mesh case.

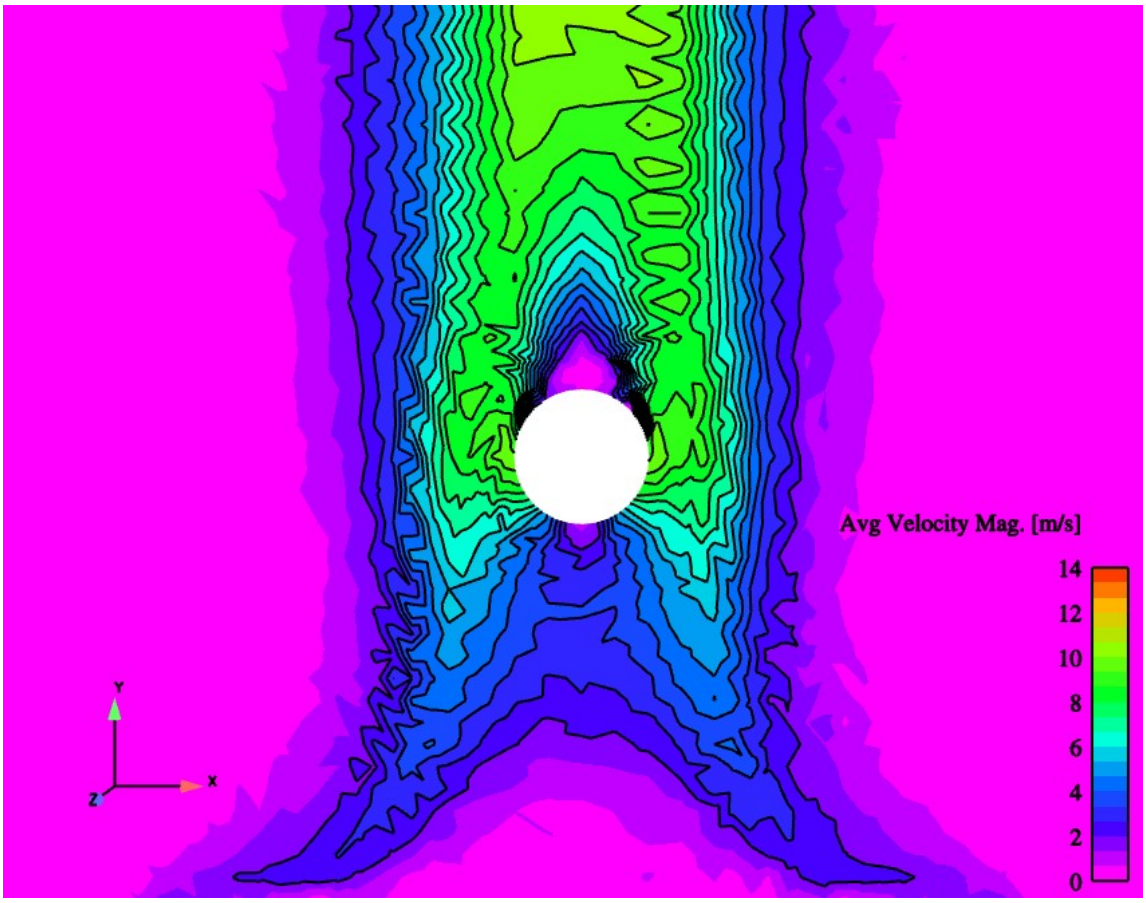

Figure A-13. Contours of the average predicted velocity magnitude.

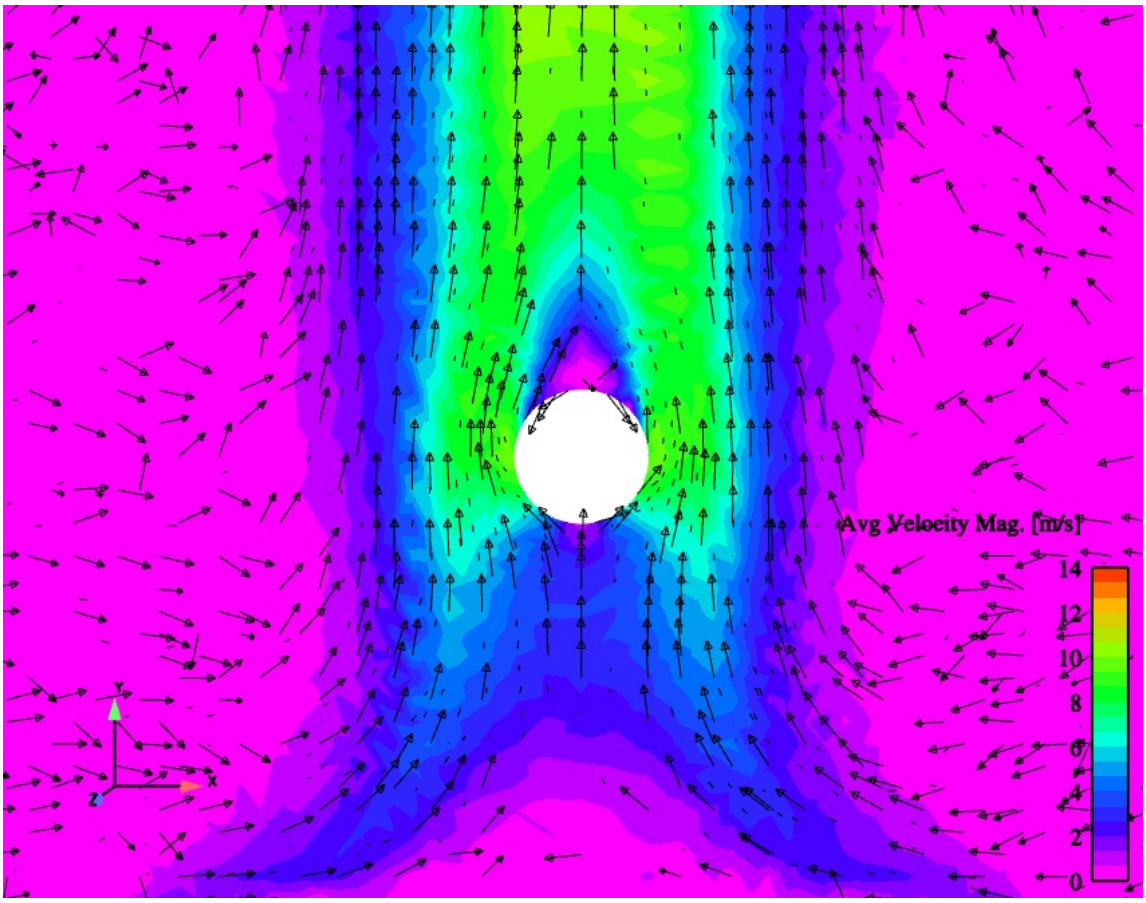

Figure A-14. Contours of the average predicted velocity magnitude with vectors overlaid.

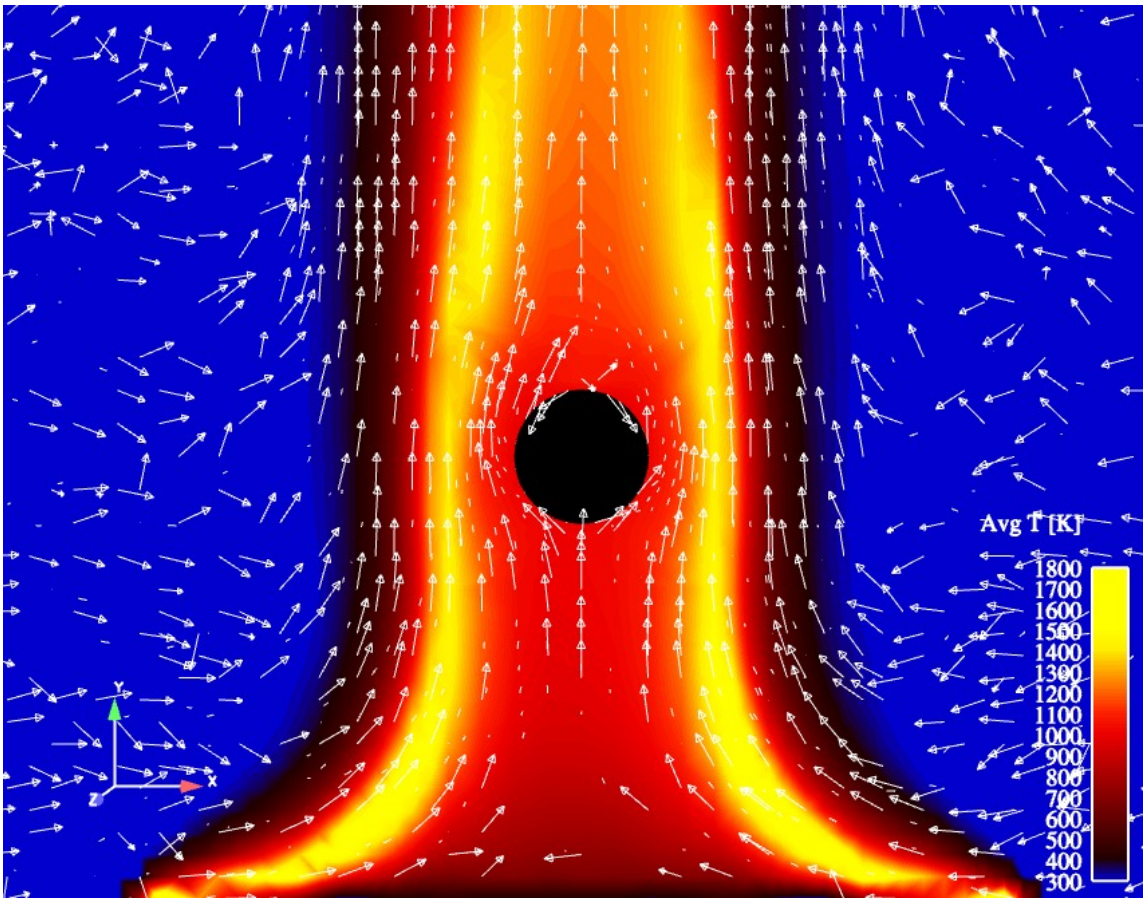

Figure A-15. Average predicted temperature at a centerplane with velocity vectors overlaid.

APPENDIX B:
APPENDIX TITLE

Manufacturer's calibration curves for the four dual (radiative and total) HFGs are included in this appendix. The locations of the HFGs are indicated on the schematic of Figure 2-12.

The gauges are referred to here as MT-1T for the total HFG of Medtherm 1 or MT-1R for the radiative HFG of Medtherm 1, as numbered in Figure 2-12. The calibration curves are included in the following order:

MT-1T
MT-1R
MT-2T
MT-2R
MT-3T
MT-3R
MT-4T
MT-4R

CERTIFICATE OF CALIBRATION

TOTAL HEAT FLUX TRANSDUCER

 HF17025_kW.DOC

DATE 7/27/04
CUSTOMER Sandia Nat'l Labs
Albuquerque, NM
P.O. NO. CC
CERTIFICATE NO. 13636-1
MODEL NO. 96-15T-15RP(ZnSe)
-21745
SERIAL NO. 136361T
SENSOR TYPE Schmidt-Boelter
ABSORPTANCE 0.94
WINDOW None
REFERENCE STANDARD 89943
CALIBRATED BY 13

CALIBRATION RESULTS SUMMARY:

FULL SCALE OUTPUT LEVEL:
10.20 mV at 150 kW/m^2

RESPONSIVITY:
0.06800 mV per (kW/m^2), or
the inverse: 14.71 kW/m^2 per mV
Water: 27.8 °C 12 mL/s

UNLESS NOTED, CALIBRATION CONDITIONS:
Non-condensing Ambient Air at 23 ±3 °C
Relative Humidity Less Than 70%
Expanded uncertainty ±3% of responsivity.
Coverage factor k=2, ~95% confidence level.
Test uncertainty ratio (TUR) is less than 4:1.

Calibration was performed in compliance with ISO/IEC 17025, ANSI/NCSL Z540-1 and MIL-STD-45662A to MEDTHERM PI-20 with traceability to the National Institute of Standards and Technology.

ATTEST:

___ QA Manager ✓ President

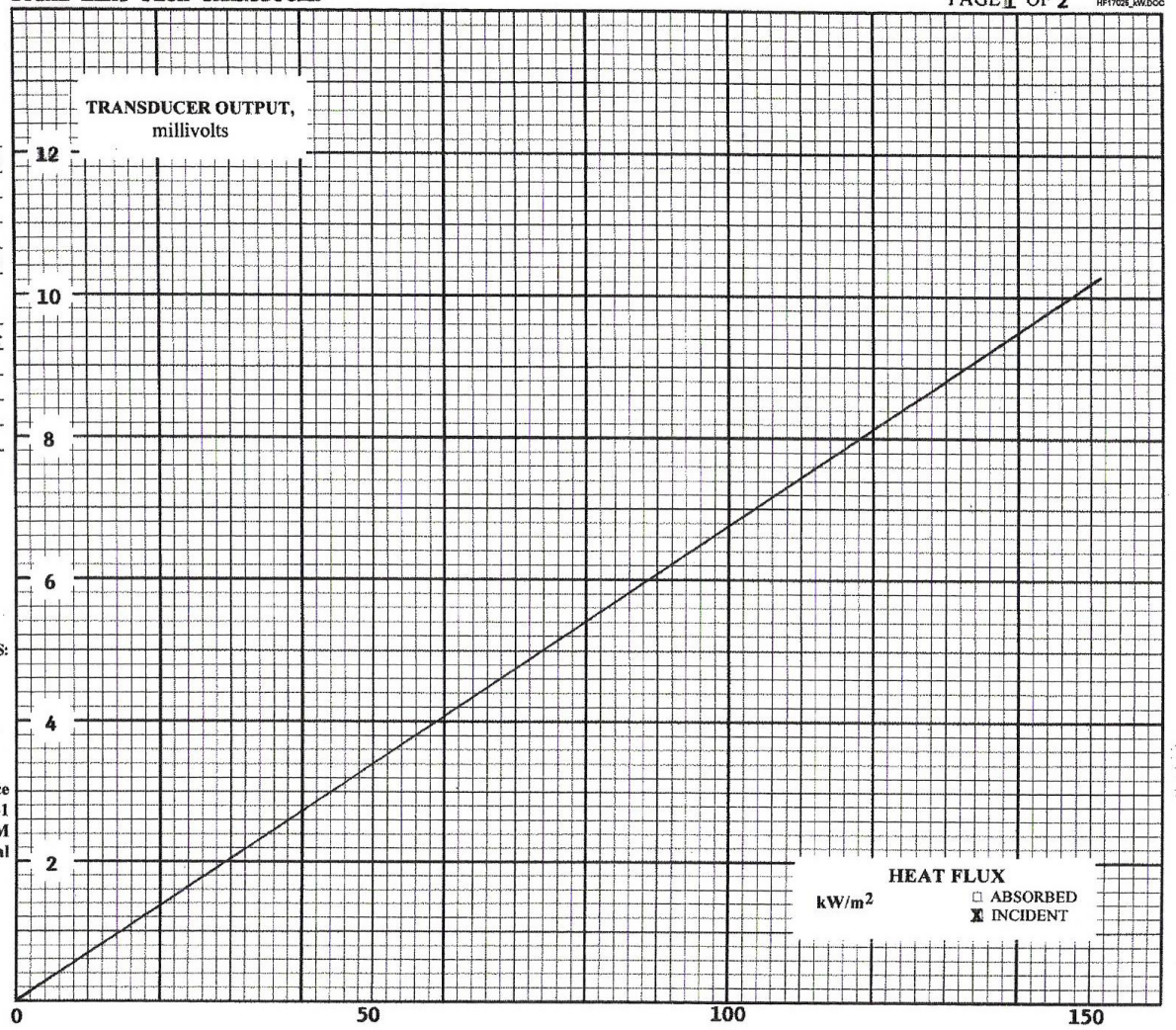

MEDTHERM
CORPORATION
POST OFFICE BOX 412 / HUNTSVILLE, ALABAMA / TELEPHONE (256) 837-2000 / FAX (256) 837-2001

RADIOMETER

 HF17025_KW.DOC

CERTIFICATE OF CALIBRATION

DATE 7/27/04
CUSTOMER Sandia Nat'l Labs
Albuquerque, NM
P.O. NO. CC
CERTIFICATE NO. 13636-1
MODEL NO. 96-15T-15RP(ZnSe)
-21745
SERIAL NO. 136361R
SENSOR TYPE Schmidt-Boelter
ABSORPTANCE 0.94
WINDOW Zinc Selenide
REFERENCE STANDARD 89943
CALIBRATED BY 13
CALIBRATION RESULTS SUMMARY:
FULL SCALE OUTPUT LEVEL:
10.23 mV at 150 kW/m^2
RESPONSIVITY:
0.06820 mV per (kW/m^2), or
the inverse: 14.66 kW/m^2 per mV
Water: 27.8 °C 12 mL/s

UNLESS NOTED, CALIBRATION CONDITIONS:
Non-condensing Ambient Air at 23 ±3 °C
Relative Humidity Less Than 70%
Expanded uncertainty ±3% of responsivity.
Coverage factor k=2, ~95% confidence level.
Test uncertainty ratio (TUR) is less than 4:1.

Calibration was performed in compliance with ISO/IEC 17025, ANSI/NCSL Z540-1 and MIL-STD-45662A to MEDTHERM PI-20 with traceability to the National Institute of Standards and Technology.

ATTEST:

____ QA Manager ✓ President

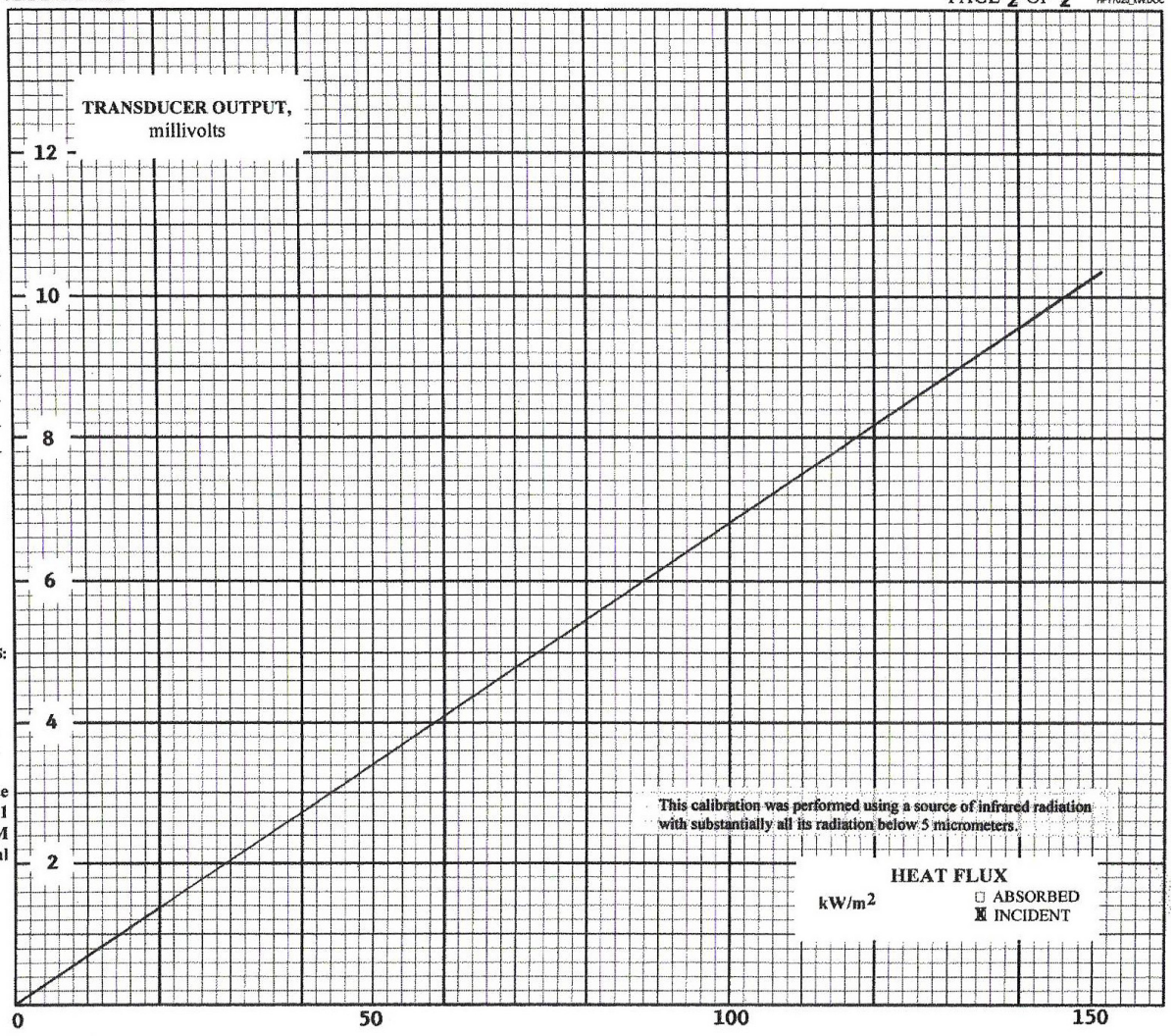

MEDTHERM
CORPORATION

POST OFFICE BOX 412 / HUNTSVILLE, ALABAMA / TELEPHONE (256) 837-2000 / FAX (256) 837-2001

TOTAL HEAT FLUX TRANSDUCER
"AS SHIPPED" CALIBRATION

Received for recalibration: 7/21/04

HF17025_WW.DOC

CERTIFICATE OF CALIBRATION

DATE 8/5/04
CUSTOMER Sandia Nat'l Labs
Albuquerque, NM
P.O. NO. CC
CERTIFICATE NO. 13638-1B
MODEL NO. 96-15T-15RP(ZnSe)
-21745
SERIAL NO. 135081T
SENSOR TYPE Schmidt-Boelter
ABSORPTANCE 0.94
WINDOW None
REFERENCE STANDARD 89943
CALIBRATED BY 6

CALIBRATION RESULTS SUMMARY:
FULL SCALE OUTPUT LEVEL:
11.52 mV at 150 kW/m^2
RESPONSIVITY:
0.0768 mV per (kW/m^2), or
the inverse: 13.02 kW/m^2 per mV
Water: 28.9 °C 11.9 mL/s

UNLESS NOTED, CALIBRATION CONDITIONS:
Non-condensing Ambient Air at 23 ±3 °C
Relative Humidity Less Than 70%
Expanded uncertainty ±3% of responsivity.
Coverage factor k=2, ~95% confidence level.
Test uncertainty ratio (TUR) is less than 4:1.

Calibration was performed in compliance with ISO/IEC 17025, ANSI/NCSL Z540-1 and MIL-STD-45662A to MEDTHERM PI-20 with traceability to the National Institute of Standards and Technology.

ATTEST: F. Beckett

X QA Manager ___ President

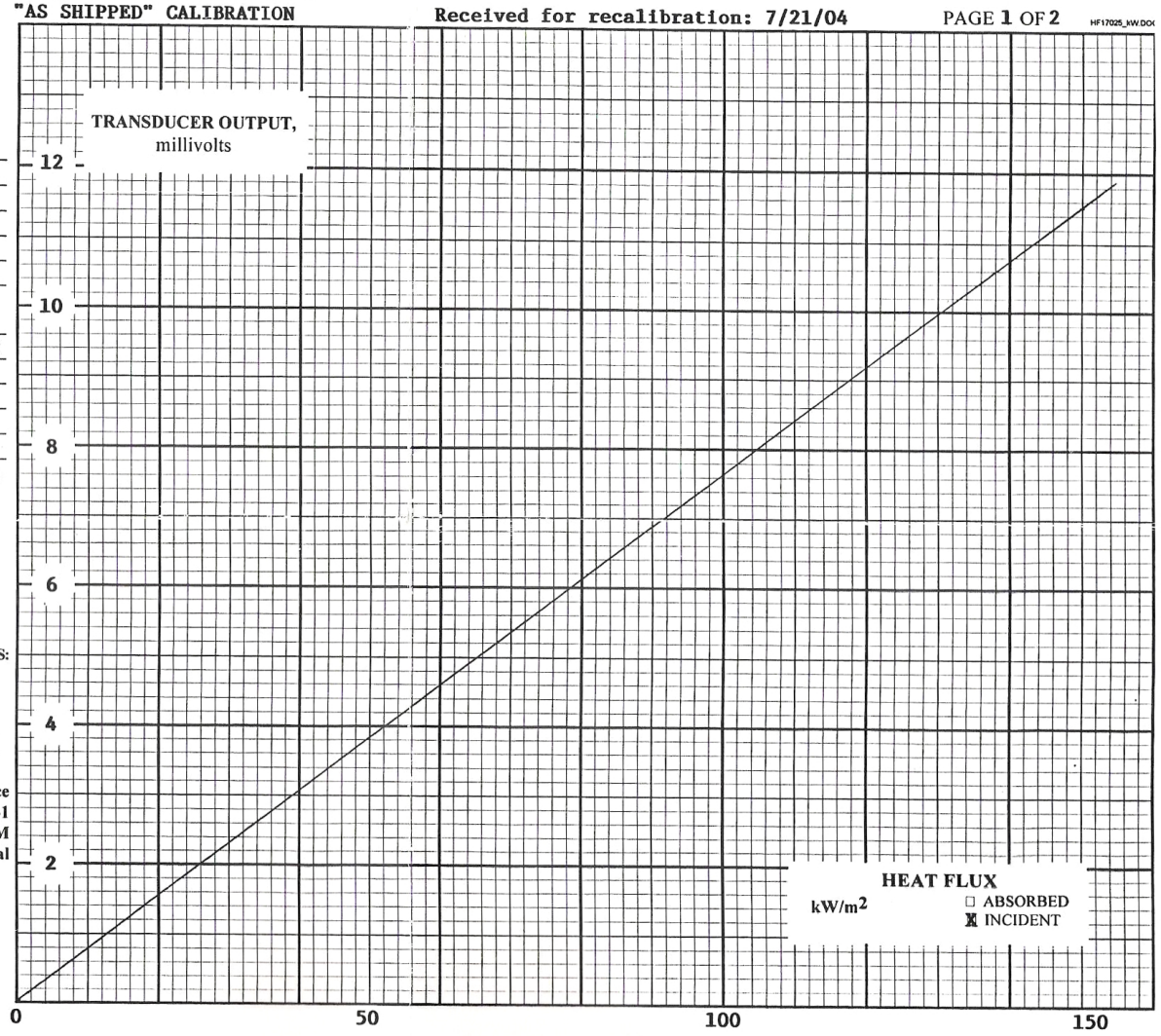

MEDTHERM
CORPORATION
POST OFFICE BOX 412 / HUNTSVILLE, ALABAMA / TELEPHONE (256) 837-2000 / FAX (256) 837-2001

CERTIFICATE OF CALIBRATION

DATE 8/5/04
CUSTOMER Sandia Nat'l Labs
Albuquerque, NM
P.O. NO. CC
CERTIFICATE NO. 13638-1B
MODEL NO. 96-15T-15RP(ZnSe)
-21745
SERIAL NO. 135081R
SENSOR TYPE Schmidt-Boelter
ABSORPTANCE 0.94
WINDOW Zinc Selenide
REFERENCE STANDARD 89943
CALIBRATED BY 6

CALIBRATION RESULTS SUMMARY:

FULL SCALE OUTPUT LEVEL:
10.36 mV at 150 kW/m^2

RESPONSIVITY:
0.06907 mV per (kW/m^2), or
the inverse: 14.48 kW/m^2 per mV
Water: 28.9 °C 11.9 mL/s

UNLESS NOTED, CALIBRATION CONDITIONS:
Non-condensing Ambient Air at 23 ±3 °C
Relative Humidity Less Than 70%
Expanded uncertainty ±3% of responsivity.
Coverage factor k=2, ~95% confidence level.
Test uncertainty ratio (TUR) is less than 4:1.

Calibration was performed in compliance with ISO/IEC 17025, ANSI/NCSL Z540-1 and MIL-STD-45662A to MEDTHERM PI-20 with traceability to the National Institute of Standards and Technology.

ATTEST: F. Beckett

X QA Manager ___ President

MEDTHERM
CORPORATION

RADIOMETER
"AS SHIPPED" CALIBRATION

Received for recalibration: 7/21/04

HF17025_kW.DOC

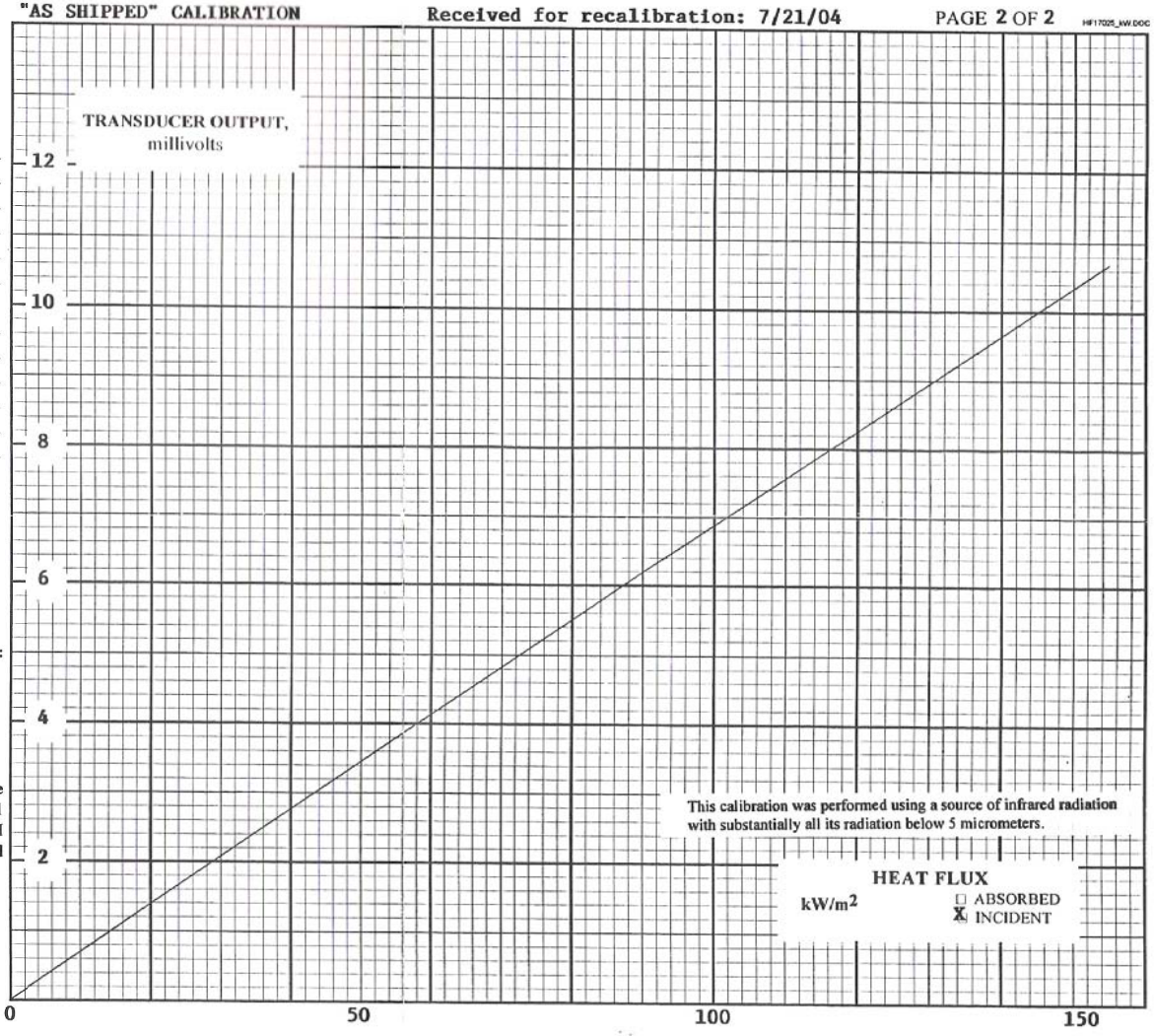

POST OFFICE BOX 412 / HUNTSVILLE, ALABAMA / TELEPHONE (256) 837-2000 / FAX (256) 837-2001

CERTIFICATE OF CALIBRATION

TOTAL HEAT FLUX TRANSDUCER

DATE 3/11/04
CUSTOMER Sandia Nat'l Labs
Albuquerque, NM
P.O. NO. CC
CERTIFICATE NO. 13481-1A
MODEL NO. 96-15T-15RP(ZnSe)
21745
SERIAL NO. 134811T
SENSOR TYPE Schmidt-Boelter
ABSORPTANCE 0.94
WINDOW None
REFERENCE STANDARD 89943
CALIBRATED BY 6

CALIBRATION RESULTS SUMMARY:
FULL SCALE OUTPUT LEVEL:
11.00 mV at 150 kW/m^2
RESPONSIVITY:
0.07333 mV per (kW/m^2), or
the inverse: 13.64 kW/m^2 per mV
Water: 15.6 °C 12.0 mL/s

UNLESS NOTED, CALIBRATION CONDITIONS:
Non-condensing Ambient Air at 23 ±3 °C
Relative Humidity Less Than 70%
Expanded uncertainty ±3% of responsivity.
Coverage factor k=2, ~95% confidence level.
Test uncertainty ratio (TUR) is less than 4:1.

Calibration was performed in compliance with ISO/IEC 17025, ANSI/NCSL Z540-1 and MIL-STD-45662A to MEDTHERM PI-20 with traceability to the National Institute of Standards and Technology.

ATTEST: F. Beckett

X QA Manager ___ President

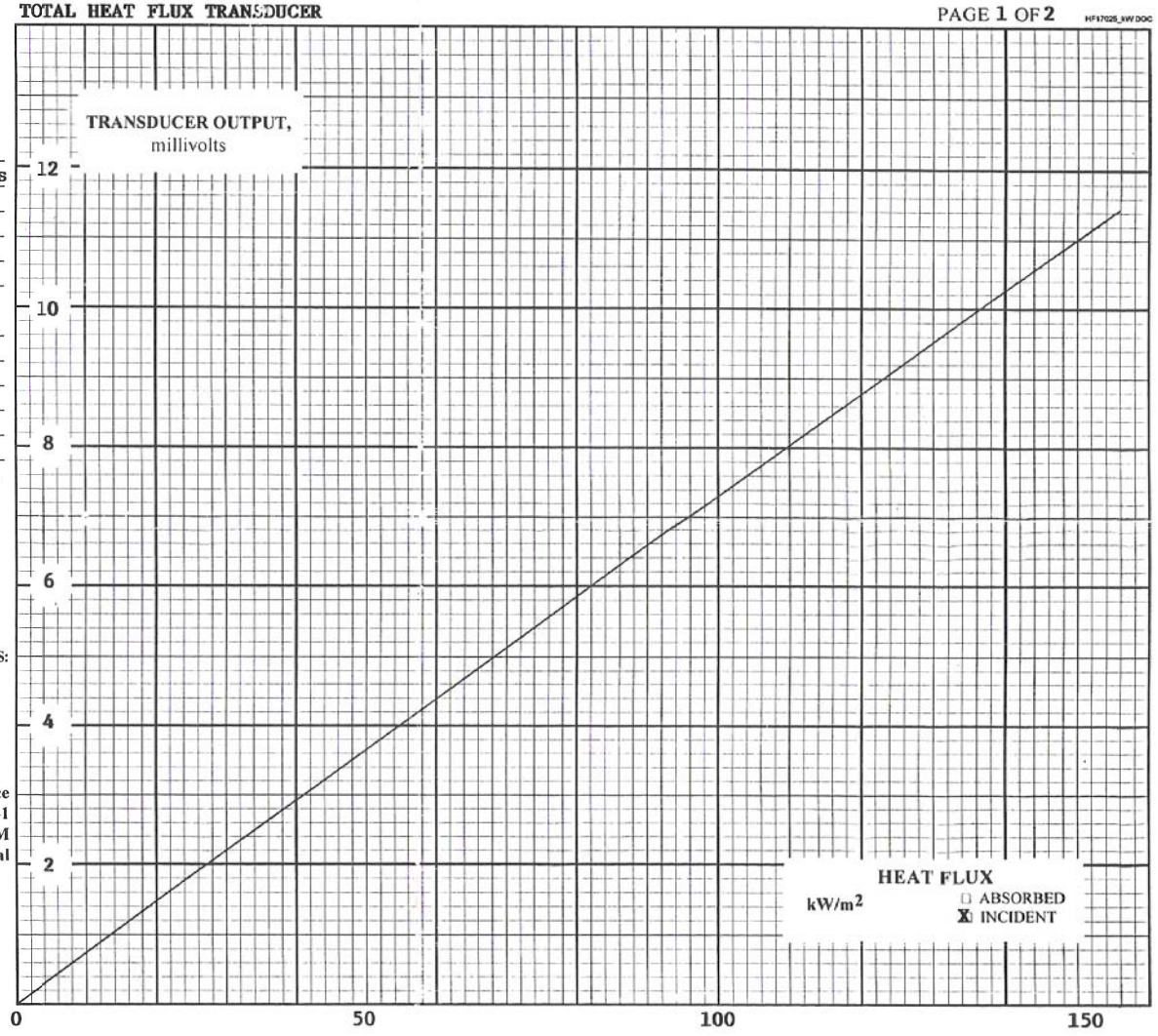

MEDTHERM
CORPORATION
POST OFFICE BOX 412 / HUNTSVILLE, ALABAMA / TELEPHONE (256) 837-2000 / FAX (256) 837-2001

RADIOMETER

CERTIFICATE OF CALIBRATION

DATE 3/11/04
CUSTOMER Sandia Nat'l Labs
Albuquerque, NM
P.O. NO. CC
CERTIFICATE NO. 13481-1B
MODEL NO. 96-15T-15RP(ZnSe)
21745
SERIAL NO. 134811R
SENSOR TYPE Schmidt-Boelter
ABSORPTANCE 0.94
WINDOW None
REFERENCE STANDARD 89943
CALIBRATED BY 6

CALIBRATION RESULTS SUMMARY:
FULL SCALE OUTPUT LEVEL:
9.47 mV at 150 kW/m^2
RESPONSIVITY:
0.06313 mV per (kW/m^2), or
the inverse: 15.84 kW/m^2 per mV
Water: 15.6 °C 12.0 mL/s

UNLESS NOTED, CALIBRATION CONDITIONS:
Non-condensing Ambient Air at 23 ±3 °C
Relative Humidity Less Than 70%
Expanded uncertainty ±3% of responsivity.
Coverage factor k=2, ~95% confidence level.
Test uncertainty ratio (TUR) is less than 4:1.

Calibration was performed in compliance with ISO/IEC 17025, ANSI/NCSL Z540-1 and MIL-STD-45662A to MEDTHERM PI-20 with traceability to the National Institute of Standards and Technology.

ATTEST: F. Beckett

X QA Manager ___ President

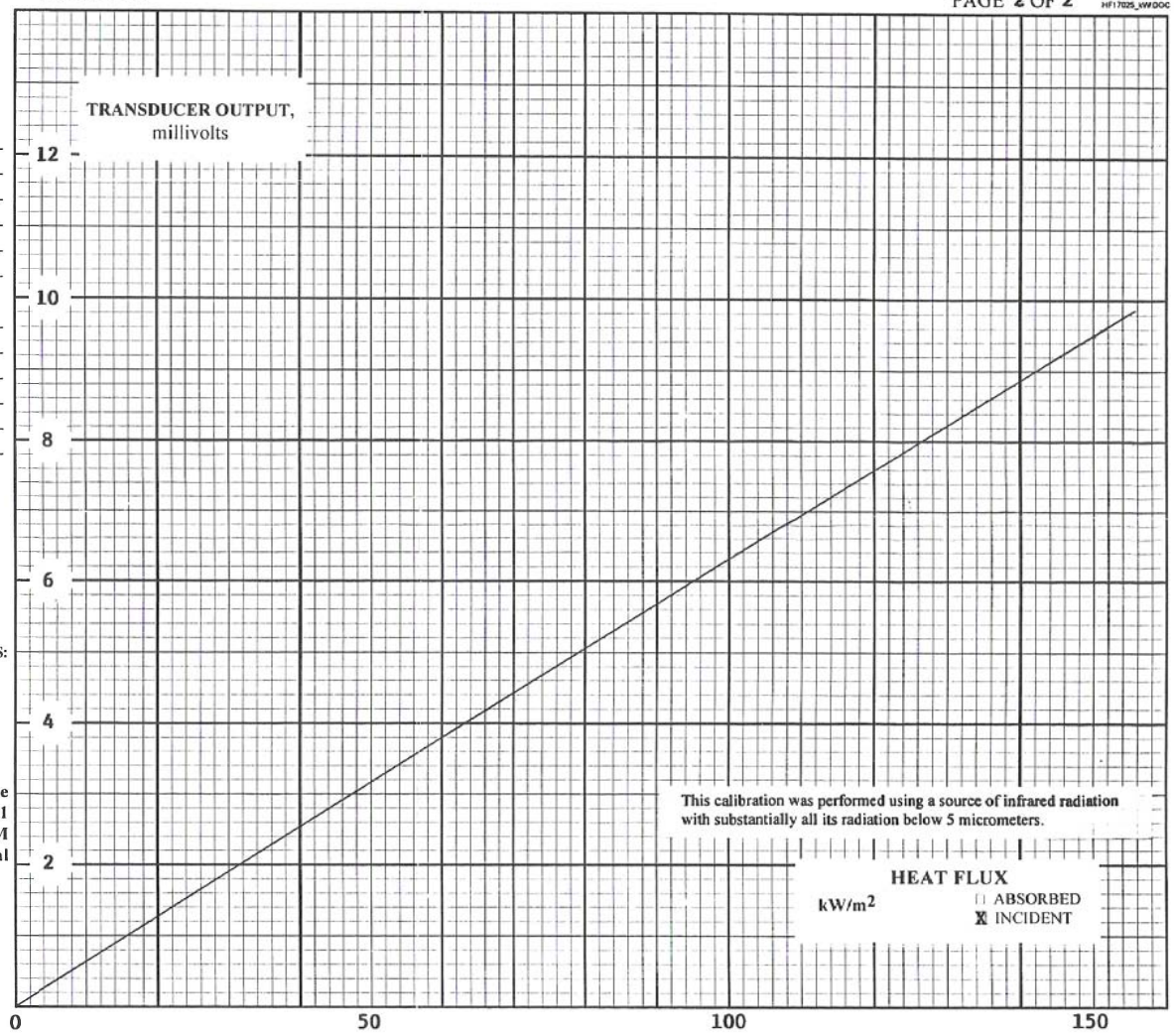

MEDTHERM
CORPORATION
POST OFFICE BOX 412 / HUNTSVILLE, ALABAMA / TELEPHONE (256) 837-2000 / FAX (256) 837-2001

ZNSEW-3-20774
(ZnSe)

TOTAL HEAT FLUX TRANSDUCER
"AS SHIPPED" CALIBRATION

Received for recalibration: 5/24/04

HF17025_WW.DOC

CERTIFICATE OF CALIBRATION

DATE 6/24/04
CUSTOMER Sandia Nat'l Labs
Albuquerque, NM
P.O. NO. CC
CERTIFICATE NO. 13567-2
MODEL NO. 96-15T-15RP(ZnSe)-21745
SERIAL NO. 134491T
SENSOR TYPE Schmidt-Boelter
ABSORPTANCE 0.94
WINDOW None
REFERENCE STANDARD 89943
CALIBRATED BY 6

CALIBRATION RESULTS SUMMARY:

FULL SCALE OUTPUT LEVEL:
10.86 mV at 150 kW/m^2

RESPONSIVITY:
0.0724 mV per (kW/m^2), or
the inverse: 13.81 kW/m^2 per mV

Water: 26.7 °C 11.8 mL/s

UNLESS NOTED, CALIBRATION CONDITIONS:
Non-condensing Ambient Air at 23 ±3 °C
Relative Humidity Less Than 70%
Expanded uncertainty ±3% of responsivity.
Coverage factor k=2, ~95% confidence level.
Test uncertainty ratio (TUR) is less than 4:1.

Calibration was performed in compliance with ISO/IEC 17025, ANSI/NCSL Z540-1 and MIL-STD-45662A to MEDTHERM PI-20 with traceability to the National Institute of Standards and Technology.

ATTEST: F. Boeckett

X QA Manager ___ President

MEDTHERM
CORPORATION

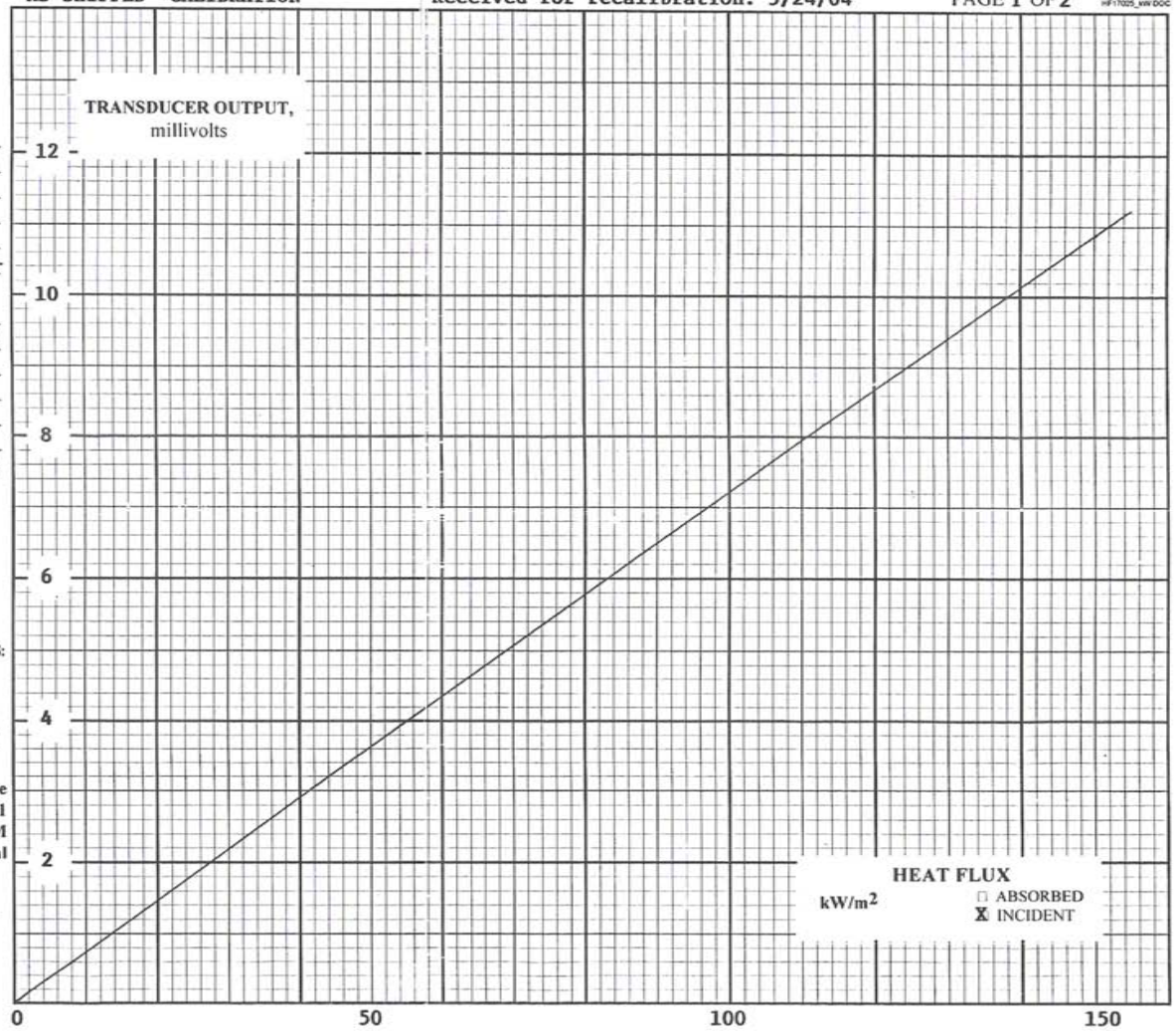

POST OFFICE BOX 412 / HUNTSVILLE, ALABAMA / TELEPHONE (256) 837-2000 / FAX (256) 837-2001

CERTIFICATE OF CALIBRATION

DATE 6/24/04
CUSTOMER Sandia Nat'l Labs
Albuquerque, NM
P.O. NO. CC
CERTIFICATE NO. 13567-2
MODEL NO. 96-15T-15RP(ZnSe)-21745
SERIAL NO. 134491R
SENSOR TYPE Schmidt-Boelter
ABSORPTANCE 0.94
WINDOW Zinc Selenide
REFERENCE STANDARD 89943
CALIBRATED BY 6
CALIBRATION RESULTS SUMMARY:
FULL SCALE OUTPUT LEVEL:
10.14 mV at 150 kW/m^2
RESPONSIVITY:
0.0676 mV per (kW/m^2), or
the inverse: 14.79 kW/m^2 per mV
Water: 26.7 °C 11.8 mL/s

UNLESS NOTED, CALIBRATION CONDITIONS:
Non-condensing Ambient Air at 23 ±3 °C
Relative Humidity Less Than 70%
Expanded uncertainty ±3% of responsivity.
Coverage factor k=2, ~95% confidence level.
Test uncertainty ratio (TUR) is less than 4:1.

Calibration was performed in compliance with ISO/IEC 17025, ANSI/NCSL Z540-1 and MIL-STD-45662A to MEDTHERM PI-20 with traceability to the National Institute of Standards and Technology.

ATTEST: F. Beckett

X QA Manager ___ President

MEDTHERM
CORPORATION

RADIOMETER
"AS SHIPPED" CALIBRATION

Received for recalibration: 5/24/04

HF17025_MW.DOC

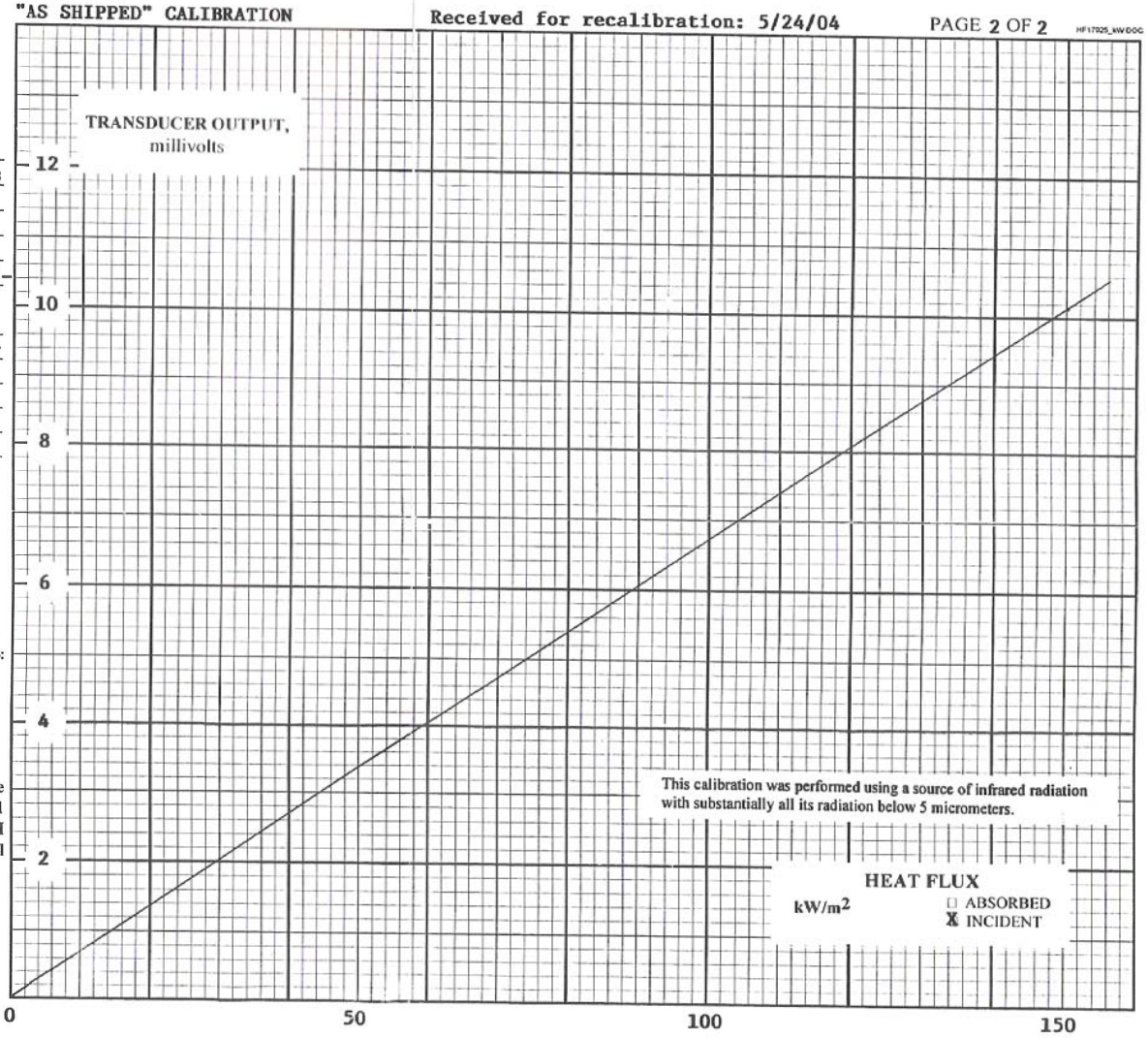

POST OFFICE BOX 412 / HUNTSVILLE, ALABAMA / TELEPHONE (256) 837-2000 / FAX (256) 837-2001

This page intentionally left blank.

DISTRIBUTION

MS0384 A.C. Ratzel, 1500
MS0824 T.Y. Chu, 1500
MS0824 W.L. Hermina, 1510
MS0821 A.L. Thornton, 1530
MS1135 T.K. Blanchat, 1532 (5)
MS0836 W. Gill, 1532
MS1135 J.T. Nakos, 1532
MS1135 A.L. Brown, 1532
MS1135 D.A. Jernigan, 1532
MS1135 A.J. Ricks, 1532
MS1135 S. Gomez, 1532
MS0836 C.A. Glissman, 1532
MS1135 S.R. Tiezsen, 1532
MS1135 J.M. Suo-Antilla, 1532
MS1135 A. Luketa-Hanlin, 1532
MS0828 M. Pilch, 1533
MS0828 V.J. Romero, 1533
MS0828 W.L. Oberkampf, 1533
MS0828 A.R. Black, 1533
MS0382 S.P. Domino, 1541
MS0834 R.D. Tachau, 1512
MS0834 T.J. O'Hern, 1512
MS0834 S.P. Kearney, 1512
MS9409 C. Moen, 8775
MS9018 Central Technical Files, 8944 (2)
MS0899 Technical Library, 4536 (2)

This page intentionally left blank.


Sandia National Laboratories